Review

Spin crossover in iron(II) complexes of 3,5-di(2-pyridyl)-1,2,4-triazoles and 3,5-di(2-pyridyl)-1,2,4-triazolates

Jonathan A. Kitchen, Sally Brooker[*]

MacDiarmid Institute for Advanced Materials and Nanotechnology and Department of Chemistry, University of Otago, PO Box 56, Dunedin, New Zealand

Contents

Abstract

The iron coordination chemistry of 3,5-di(2-pyridyl)-1,2,4-triazoles and 3,5-di(2-pyridyl)-1,2,4-triazolates is reviewed. This includes both mononuclear and dinuclear complexes, and both iron(II) and iron(III) oxidation states. The main focus is on the synthesis, structure and magnetic properties of these complexes.
© 2007 Elsevier B.V. All rights reserved.

Keywords: Spin crossover; Iron; Triazole; Structure; Synthesis; Magnetism

* Corresponding author. Tel.: +64 3 479 7919; fax: +64 3 479 7906.
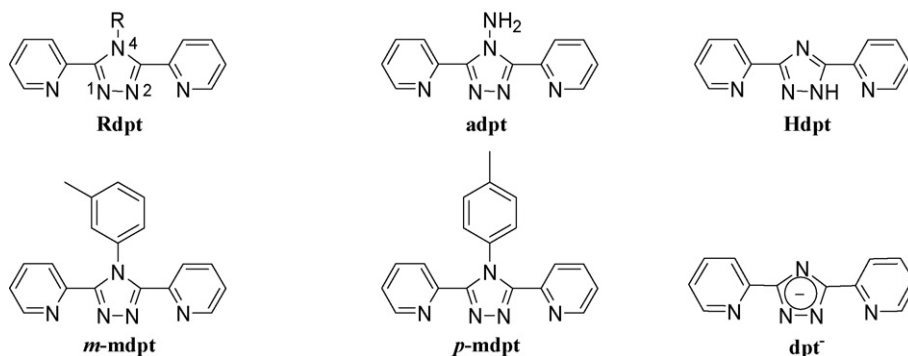 *E-mail address:* sbrooker@chemistry.otago.ac.nz (S. Brooker).

Fig. 1. A general schematic representation of a 3,5-di(2-pyridyl)-1,2,4-triazole (**Rdpt**) along with the only 3,5-di(2-pyridyl)-1,2,4-triazoles (**adpt**, **Hdpt**, *m*-**mdpt**, *p*-**mdpt**) and 3,5-di(2-pyridyl)-1,2,4-triazolate (**dpt⁻**) for which iron complexes have been structurally characterized.

1. Introduction

1.1. Spin crossover

The phenomenon of spin crossover (SCO) is quite frequently observed in complexes containing iron(II) with an N_6 coordination sphere [1–6]. Research into the preparation and properties of complexes that exhibit this effect has been extensive due to potential applications such as molecular switches and memory devices [7]. To induce SCO in these complexes the ligands must impose a ligand field strength that results in a minimal difference between the octahedral splitting energy (Δ_O) and the electron spin pairing energy (P) such that a minor perturbation results in switching between the high-spin [HS] ($S = 2$) and low-spin [LS] ($S = 0$) states of the iron(II) centre. Ligands based around 1,2,4-triazole moieties often meet these requirements [5]. An advantage of this azole is that the substituents at the C^3, N^4 and C^5 positions can be relatively
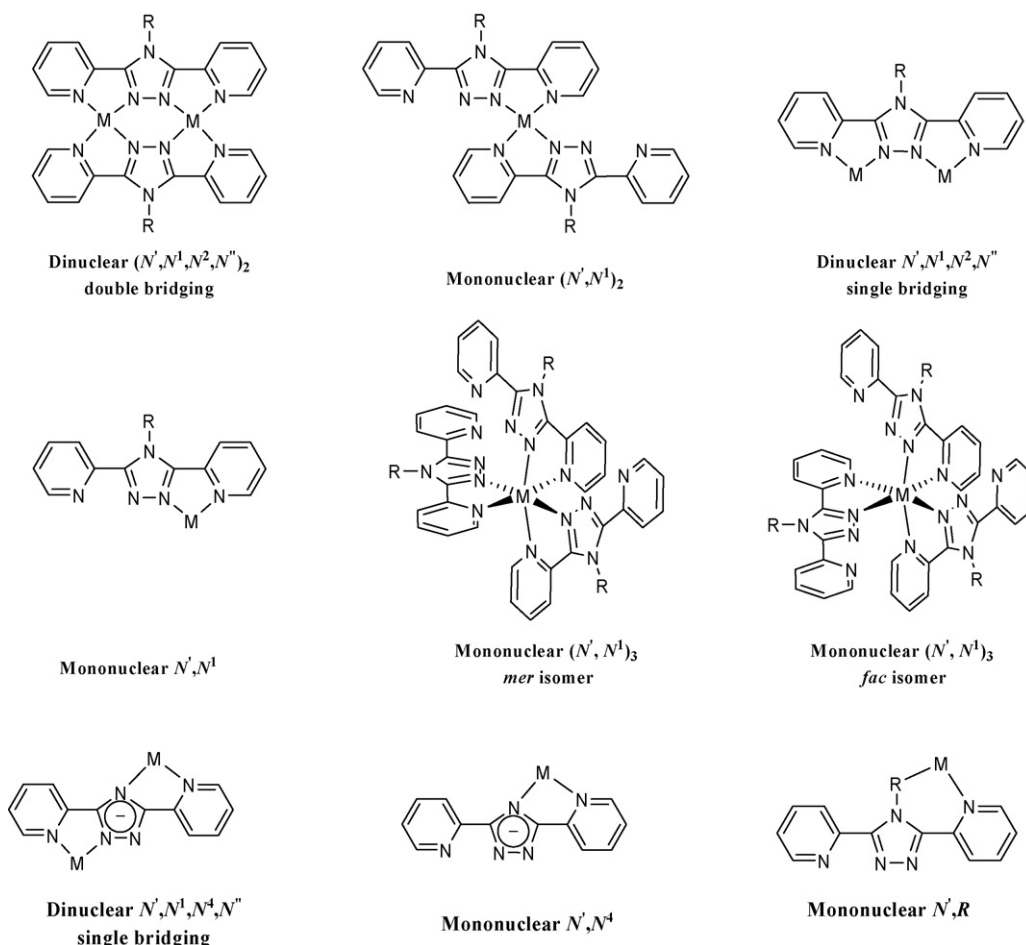

Fig. 2. Binding modes observed to date for complexes, of any metal ion, of 3,5-di(2-pyridyl)-1,2,4-triazoles and 3,5-di(2-pyridyl)-1,2,4-triazolates. Of these, only the mononuclear N',N^1, mononuclear $(N',N^1)_2$ and dinuclear $(N',N^1,N^2,N'')_2$ double bridging modes have been observed to date for complexes of iron.

Table 1
Summary of information on the iron complexes of 3,5-di(2-pyridyl)-1,2,4-triazoles/triazolates
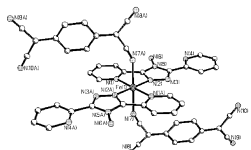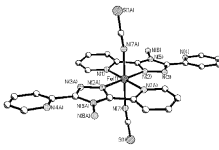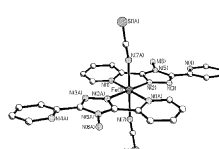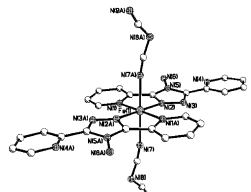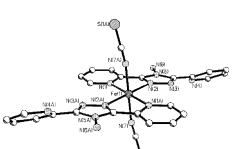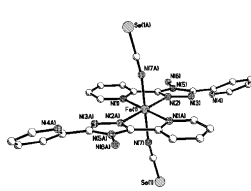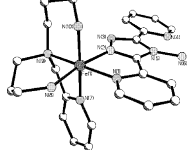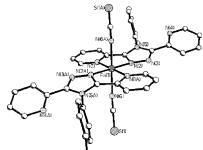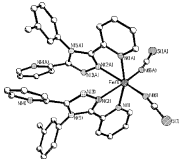
Complex	Binding mode	Structure	Space group	Colour of single crystal	Yield[a] (%)	Oxidation state	Spin state	$T_{1/2}$ (K)	References
[Fe(**abpt**)$_2$(TCNQ)$_2$]	Mono. bis		P-1	Black	NR	2+	SCO	280	[61]
[Fe(**abpt**)$_2$(NCS)$_2$]	Mono. bis		$P2_1/n$	Red	NR	2+	SCO	180	[42]
[Fe(**abpt**)$_2$(NCSe)$_2$]	Mono. bis		$P2_1/n$	Red	NR	2+	SCO	224	[42]
[Fe(**abpt**)$_2$(N(CN)$_2$)$_2$]	Mono. bis		P-1	Orange	50	2+	SCO	84	[33]
[Fe(**abpt**)$_2$(NCS)$_2$]	Mono. bis		$P2_1/n$	Orange	60	2+	SCO[b]	HS (1 bar) 65 (4.4 bar) 106 (5.6 bar) 152 (8.6 bar) 179 (10.5 bar)	[43]
[Fe(**abpt**)$_2$(NCSe)$_2$]	Mono. bis		$P2_1/n$	Orange	60	2+	HS	N/A	[43]
[Fe(**abpt**)(DAPP)]$^{2+}$	Mono.		$P2_1/n$	Yellow-brown	NR	2+	SCO (hysteresis)	171↓ 181↑	[34]
[Fe(**abpt**)(tren)]$^{2+}$	Mono.[c]	N/A	N/A	Dark Brown	55	2+	HS[d]	N/A[d]	[45]
[Fe(**abpt**)(trpn)]$^{2+}$	Mono.[c]	N/A	N/A	Brown	50	2+	SCO	NR[e]	[28]
[Fe(**p-mbpt**)$_2$(NCS)$_2$]	Mono. bis		P-1	Red-brown	91	2+	SCO	231	[30]

Table 1 (*Continued*)

Complex	Binding mode	Structure	Space group	Colour of single crystal	Yield[a] (%)	Oxidation state	Spin state	$T_{1/2}$ (K)	References
[Fe(***m*-mbpt**)$_2$(NCS)$_2$]	Mono. bis		*C*2/*c*	Red	85	2+	HS	N/A	[30]
[Fe(**Hbpt**)Cl$_3$(H$_2$O)]	Mono.		*P*-1	Red	54	3+	HS	N/A	[46]
[Fe$_2$(**bpt**$^-$)$_2$Cl$_4$]	Di. bis		*Pnnm*	Purple	82	3+,3+	HS-HS	N/A	[46]
[Fe$_2$(**bpt**$^-$)$_2$(MeOH)$_2$Cl$_2$]	Di. bis		*Pbca*	Yellow	79	2+,2+	HS-HS	N/A	[46]
[Fe$_2$(**bpt**$^-$)$_2$(py)$_2$(NCS)$_2$]	Di. bis		*P*2$_1$/*n*	Yellow	66	2+,2+	HS-HS	N/A	[64]
[Fe$_2$(**bpt**$^-$)$_2$(py)$_2$(NCSe)$_2$]	Di. bis [c]	N/A	N/A	Yellow	39	2+,2+	HS-HS	N/A	[64]
[Fe$_2$(**bpt**$^-$)$_2$(py)$_2$(NCBH$_3$)$_2$]	Di. bis [c]	N/A	N/A	Orange	42	2+,2+	2 step SCO	T_1 = 194 K T_2 = 151 K	[64]

[a] NR = not reported.

[b] The sample displays SCO at elevated pressures. At ambient pressure it is HS.

[c] The exact binding mode cannot be confirmed as there is no crystal structure, however sporting methods and comparisons to crystal structures of other first row transition metal ions with the same ligand system led to the proposed binding mode.
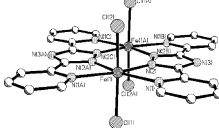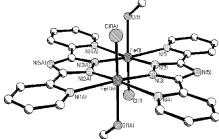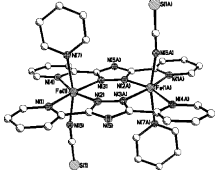
[d] Only a 298 K magnetic moment was reported. In the absence of VT data it is unknown whether or not it is SCO active.

[e] Although the sample is SCO active, HS at 298 K and LS at 80 K, a full VT run was not carried out so $T_{1/2}$ is unknown.

easily altered, giving access to triazole-based ligands with a wide range of dentisity, solubility, steric and electronic properties [5,8–12], which in turn opens up access to rich and diverse families of iron(II) coordination compounds [5,9,13].

This review covers the synthesis, structures and properties of the iron(II) complexes of ligands in which there is a 2-pyridyl group at both the C^3 and C^5 positions of the 1,2,4-triazole moiety, i.e. the 3,5-di(2-pyridyl)-1,2,4-triazoles (with a variety of N^4 substituents) and 3,5-di(2-pyridyl)-1,2,4-triazolates (Fig. 1, Table 1). The main focus of this review is on those complexes which have been structurally characterized. Interestingly, to date only one structurally characterized complex (of copper) exists in which any of the 2-pyridyl rings contain an additional substituent, in that case a methyl group at the 3-position of one of the two rings [14]. Related iron complexes, of 3-(2-pyridyl)-1,2,4-triazole [15], 3-(2-pyridyl)-1,2,4-pyrazole [16,17] and 3,5-di(2-pyridyl)-1,2,4-pyrazole [18], are not included here.

1.2. Binding modes

Each 3,5-di(2-pyridyl)-1,2,4-triazole/triazolate ligand strand contains two bidentate binding pockets that are each capable of forming a five membered chelate ring with a metal centre (Fig. 2). Various discrete dinuclear complexes are possible. Depending on whether the product has an M:L ratio of 2:1 or 2:2 the iron(II) centres will be either singly or doubly bridged by the triazole/triazolate. The singly bridged group can be further subdivided. In principle an N^1N^2 bridging mode is possible for both N^4-substituted and N^4-unsubstituted ligands. In the case of N^4-unsubstituted ligands binding can also occur via N^4, giving rise to N^1N^4 bridging of the two metal ions. In summary, three possible dinuclear binding modes are readily identifiable (Fig. 2): N',N^1,N^2,N'' single bridging, N',N^1,N^4,N'' single bridging and dinuclear $(N',N^1,N^2,N'')_2$ double bridging (also known as dinuclear bis complexes) by the di(2-pyridyl)-1,2,4-triazole/triazolate ligand(s).

A range of mononuclear complexes, in which only one of the two possible binding sites is occupied by a metal ion, are also possible (Fig. 2). Examples of M:L ratio in such products include 1:1, 1:2 and 1:3. These correspond to the mononuclear N',N^1, mononuclear $(N',N^1)_2$ (also known as mononuclear bis complexes) and $(N',N^1)_3$ (also known as the tris complexes) as well as the analogous $(N',N^4)_n$ set ($n = 1$–3) which is also possible for the N^4-unsubstituted ligand. Two geometrical isomers are possible for the tris complexes, *facial* or *meridional* (Fig. 2), and one must also remember that there will be optical isomers to consider in these cases. To date, no tris complexes have been seen for 3,5-di(2-pyridyl)-1,2,4-triazole/triazolate complexes [19], however, 3-(2-pyridyl)-1,2,4-triazoles have generated tris complexes [15,20].

In principle, a variety of polymeric species are also possible, however, only 5 such species have been structurally characterized for this ligand family to date: all involve triazolate ligands and copper ions [21–23]. Other possible binding modes include those in which the N^4 substituent also contains a donor atom. This is rare but occurs in the case of 4-amino-3,5-di(2-pyridyl)-1,2,4-triazole (**adpt**) where binding can occur via the amino N^4-substituent and a pyridine nitrogen, the mononuclear N'R binding mode (Fig. 2).

Of this wide range of possible 3,5-di(2-pyridyl)-1,2,4-triazole/triazolate ligand binding modes (Fig. 2) the mononuclear bis $(N',N^1)_2$ (30 examples) and dinuclear bis $(N',N^1,N^2,N'')_2$ double bridging (18 examples) are the most common amongst the 76 structurally characterized transition metal complexes reported to date [21–64]. The next most common binding mode observed to date is the mononuclear mono-ligand (N',N^1 and N',N^4) (14 examples). Of the mononuclear mono-ligand complexes there is only one containing a N',N^4 configuration: while this cadmium(II) complex is actually dimeric due to two chloride bridges between the cadmium ions, the binding mode of the 3,5-di(2-pyridyl)-1,2,4-triazole ligand to cadmium is N',N^4 [62].

The next most common group of complexes is polynuclear, with eight examples. These include the five polymeric species mentioned above as well as some tetranuclear grid/square complexes. The actual binding modes of the ligands in these complexes are of a dinuclear type, however, we have concluded that it is appropriate to separate these complexes from the discrete dinuclear ones on the basis that these contain multiple metal centres and hence the overall type of bridging observed is different [14,21–23,49]. All of these polymeric complexes contain unsubstituted triazolate ligands, and all contain copper [Cu(I) and Cu(II)] as the metal centre. Of the polymeric complexes only one structure has M–N bonds to all three of the triazolate nitrogen atoms, making it the only one if its kind ($N^1N^2N^4$ single bridging) to date [23].

Discrete dinuclear mono-ligand (N',N^1,N^2,N'' single bridging, N',N^1,N^4,N'' single bridging) are less common binding modes, with only four structurally characterized examples. Of these only one contains the N',N^1,N^2,N'' single bridge binding mode [59], and three the N',N^1,N^4,N'' single bridge binding mode [37,51].

The remaining binding mode to be observed amongst these 76 structures is the rare mononuclear N'R binding mode (Fig. 2), observed for just two[1] triazole-based complexes. These both involve **adpt** binding via the amino N^4-substituent and a pyridine nitrogen (N') to a second row transition metal ion, Rh(III) or Ru(II). To date this mode has not been reported for any first row transition metal ion. The Rh(III) complex contains a deprotonated **adpt** ligand (i.e. NH$^-$ rather than NH$_2$ is bound to the metal centre) [39] while for the Ru(II) complex this deprotonation is not observed [55].

Initial studies aimed at establishing control of the binding mode observed in the product have shown that while the stoichiometry of the reaction can influence this, other factors, such as the electronic/steric effect of the N^4 substituent, the relative solubilities of the many and various possible products (also influenced by the N^4 substituent) and the relative concentrations in solution, also play a part in determining the nature of the solid products obtained [36,57,63]. These studies targeted the formation of dimetallic complexes and resulted in the first families of structurally characterized dinuclear $(N',N^1,N^2,N'')_2$ double bridging complexes. The metal ions employed were cobalt(II), nickel(II), copper(II) and zinc(II). Prior to these studies, the structure of $[Co_2^{II}(L)_2(OH_2)_4]^{4+}$, where L is 4-(1-pyrrolyl)-3,5-di(2-pyridyl)-1,2,4-triazole, had been reported [38].

Of the 76 structures mentioned above, 19 contain 3,5-di(2-pyridyl)-1,2,4-tri<u>azolate</u> ligands while the remaining 57 contain 3,5-di(2-pyridyl)-1,2,4-tri<u>azole</u>-based ligands. Of these 76 structurally characterized transition metal complexes only 13 contain iron: specifically there are 11 iron(II) and 2 iron(III) complexes. These 13 iron complexes, along with some other, not-yet-structurally-characterized, *iron* complexes of *3,5-di(2-pyridyl)-1,2,4-triazole/triazolate* ligands are the focus of this review. Interestingly, the only binding modes reported to date for such iron complexes are the mononuclear N',N^1, mononuclear bis$(N',N^1)_2$ and dinuclear bis$(N',N^1,N^2,N'')_2$ double bridging modes (Fig. 2). Given the difficulties we have experienced in isolating a complex of a pre-selected di(2-pyridyl)-1,2,4-triazole binding mode (see above) [36,57,63], and of the importance (whether or not its present in the product) of solvent on the magnetic behaviour of the resulting complex (see later), synthetic details are provided, along with an analysis of the structure and magnetic behaviour of each of these complexes.

2. N^4-substituted-3,5-di(2-pyridyl)-1,2,4-triazole ligands

2.1. Introductory remarks

All of the structurally characterized iron complexes of N^4-substituted 3,5-di(2-pyridyl)-1,2,4-triazole ligands are of iron(II). In contrast to the variety of binding modes observed

---

[1] A search of the CCDC initially revealed three such structures, however after XIJWUI was published it was realized that the crystal structure was incorrectly reported and that the proposed formation of an N–O bond at the N^4 position in **Hdpt** during complexation with Rh(III), was incorrect. Instead the complex was simply of **adpt**, as this was later found to be present as a major impurity in the sample of **Hdpt** used.

with other transition metal ions (Fig. 2), all bar one of these complexes are neutral mononuclear bis complexes [mononuclear (N',N^1)$_2$], [Fe^{II}L$_2$X$_2$], with an N$_6$ octahedral coordination sphere comprising two (neutral) bidentate di(2-pyridyl)-triazoles and two N-bound anionic co-ligands, e.g. NCS, NCSe, dicyanamide and TCNQ. The exception to this is the mononuclear N',N^1 mode seen in [Fe^{II}L(DAPP)](ClO$_4$)$_2$, in which a tetradentate non-triazole ligand (DAPP) is bound in addition to the (neutral) bidentate di(2-pyridyl)-triazole **adpt** (see Section 2.2.3).

All but two of these structurally characterized iron complexes utilize the triazole-based ligand 4-amino-3,5-di(2-pyridyl)-1,2,4-triazole (**adpt**, Fig. 1) in which the N^4 substituent is an amino group [8]. The other two iron complexes have a di(2-pyridyl)-triazole ligand with a *meta*-tolyl or *para*-tolyl N^4 substituent (**m-mdpt** and **p-mdpt**, Fig. 1) [44].

2.2. Complexes of 4-amino-3,5-di(2-pyridyl)-1,2,4-triazole (adpt)

2.2.1. [Fe^{II}(adpt)$_2$(TCNQ)$_2$]

Haasnoot and co-workers reported the first structurally characterized iron(II) complex of a di(2-pyridyl)-triazole, [Fe^{II}(**adpt**)$_2$(TCNQ)$_2$]. It featured the radical anion 7,7′,8,8′-tetracyanoquinodimethane (TCNQ) as the axial co-ligands [61]. A stoichiometric reaction (1:2:2) between Fe(TsO)$_2$·6H$_2$O, **adpt** and LiTCNQ, in methanol at room temperature under nitrogen was employed. Initially the solutions of Fe(II) and **adpt** were mixed before the addition of the solution of LiTCNQ. Black microcrystals formed immediately. Repeating the reaction in boiling methanol allowed X-ray quality (single) shiny black plate-like crystals to form.

The magnetic susceptibility of this black complex was measured over the temperature range 7–450 K and a gradual, almost complete, spin state transition observed (Fig. 3). The effective magnetic moment, 5.44μ_B (χT = 3.70 cm^3 mol^{-1} K) at 450 K, started dropping at about 340 K and by 7 K was 1.41μ_B (χT = 0.25 cm^3 mol^{-1} K). The transition temperature ($T_{1/2}$), which is defined as the temperature at which there is a 50:50 mixture of HS:LS in the sample, was about 280 K and the
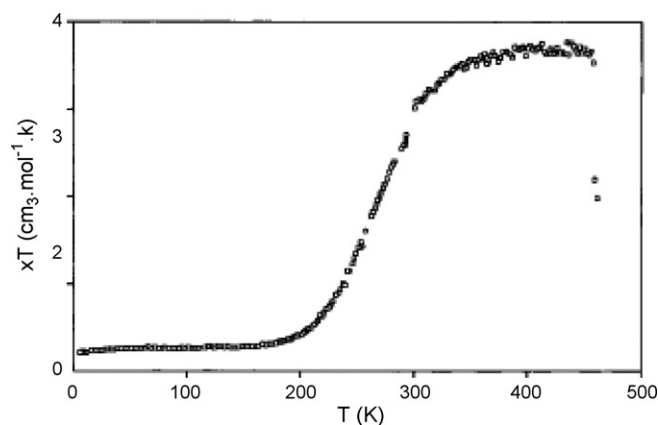

Fig. 3. Plot of variable temperature magnetic data for [Fe^{II}(**adpt**)$_2$(TCNQ)$_2$]. Reprinted with permission from J. Am. Chem. Soc. 118 (1996) 2190. Copyright 1996, American Chemical Society.

temperature range over which this gradual transition occurred was ~340–200 K. The value of 1.41μ_B at 7 K indicated that either there is incomplete SCO or there is a small paramagnetic contaminant. A 7% contamination by residual HS iron(II) was considered but the Mössbauer data were not consistent with the presence of such species. Rather the Mössbauer data showed, along with the typical signals for a temperature dependant SCO event, a signal consistent with the presence of HS iron(III) in a trace amount (it was reported that 3% iron(III) contaminant could give rise to such a spectrum). This possibility would explain not only the enhanced μ_{eff} observed at 7 K, but also the μ_{eff} observed at 450 K, as 5.44μ_B is at the upper limit of the range expected for HS iron(II).

The single crystal X-ray structure of [Fe^{II}(**adpt**)$_2$(TCNQ)$_2$] was determined at both 298 K (iron(II) primarily in the HS state, Fig. 4) and 100 K (all iron(II) in the LS state). Both structures were found to be in the *P*-1 space group with one mononuclear complex in the unit cell and hence the iron(II) ion located on a center of inversion. The volume of the cell increased by just 3.6% from 100 to 298 K. As expected the structures differ primarily in the bond lengths and angles at the distorted octahedral iron(II) centre (Table 2).
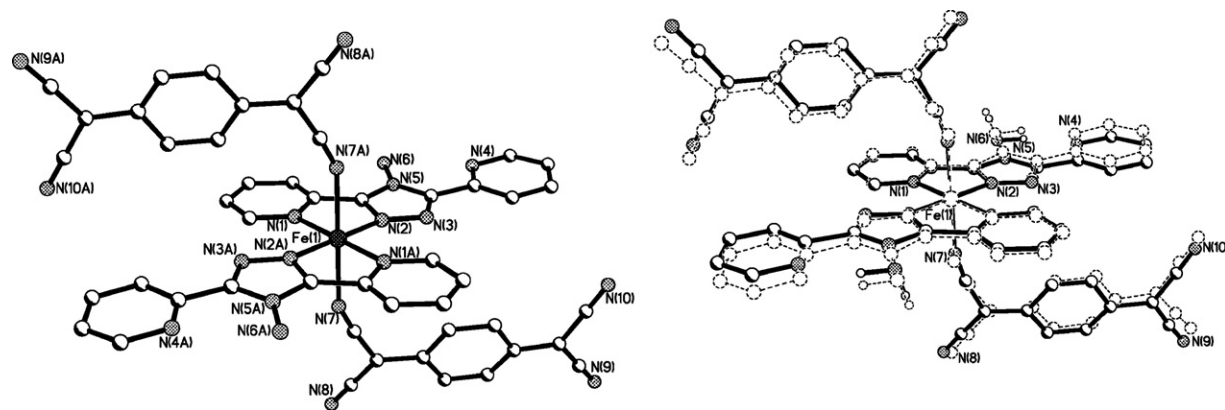
Fig. 4. Structure of [Fe^{II}(**adpt**)$_2$(TCNQ)$_2$] at: (LHS) 298 K with iron(II) primarily in the HS state; and (RHS) 100 K structure in solid lines, with all iron(II) in the LS state, overlaid with the 298 K structure in dotted lines by fitting the atoms N(1), N(2), N(1A), N(2A) and Fe(1). Symmetry operation to generate equivalent atoms: (A) −x, −y, −z. These figures were generated from data obtained from the Cambridge Crystallographic Data Centre as published originally in [61].

Table 2
Reported colours, bond lengths and angles for some of the structurally characterized iron(II) complexes of 4-amino-3,5-di(2-pyridyl)-1,2,4-triazole (i.e. L = **adpt**)

Bond lengths (Å) and angles (°)	[Fe(**L**)$_2$(TCNQ)$_2$] 298 K black	[Fe(**L**)$_2$(TCNQ)$_2$] 100 K black	[Fe(**L**)$_2$(N(CN)$_2$)$_2$] 293 K orange	[Fe(**L**)$_2$(NCS)$_2$] 293 K red polymorph	[Fe(**L**)$_2$(NCSe)$_2$] 293 K red polymorph	[Fe(**L**)$_2$(NCS)$_2$] 293 K orange polymorph	[Fe(**L**)$_2$(NCSe)$_2$] 293 K orange polymorph
Fe–N$_P$	2.12(1)	2.02(1)	2.216(2)	2.205(5)	2.189(8)	2.226(4)	2.217(5)
Fe–N$_T$	2.08(1)	2.00(2)	2.121(2)	2.120(4)	2.105(8)	2.162(4)	2.171(5)
Fe–N$_X$	2.16(1)	1.93(1)	2.160(2)	2.120(5)	2.131(9)	2.125(5)	2.120(5)
N$_T$–Fe–N$_P$	77.2(5)	80.3(6)	75.17(6)	75.0(2)	74.9(3)	75.18(14)	74.8(2)
N$_T$–Fe–N$_P$*	102.8(5)	99.7(6)	104.8	105.0(2)	105.1(3)	104.8	105.2
N$_T$–Fe–N$_X$	91.5(5)	87.3(6)	89.10(6)	87.5(2)	87.7(3)	86.8(2)	86.9(2)
N$_T$*–Fe–N$_X$	88.5(5)	92.7(6)	90.9	92.5(2)	92.3(3)	93.2	93.4
N$_X$–Fe–N$_P$	88.3(5)	92.2(6)	90.28(6)	89.8(2)	89.4(3)	89.2(2)	88.9(2)
N$_X$–Fe–N$_P$*	91.7(5)	87.8(6)	89.7	90.2(2)	90.6(3)	90.8	91.1
Fe–N$_X$–C$_X$	151(1)	162(1)	165.9	167.2(5)	169.7(10)	169.6(4)	169.7(5)
Symmetry operation used to generate equivalent atoms (*)	−x, −y, −z	−x, −y, −z	−x, −y+1, −z	−x, −y+1, −z	−x, −y+1, −z	−x, −y, −z	−x, −y, −z+1

N$_P$ = coordinated pyridine ring nitrogen atom, N$_T$ = coordinated triazole ring nitrogen atom, N$_X$ = axial substituent nitrogen atom, Fe–N$_X$–C$_X$ = angle formed between axial co-ligand and the iron(II) center.

At 298 K the bond lengths and angles between the iron(II) centre and the coordinated nitrogen atoms are consistent with those of a HS iron(II) complex, while at 100 K the structure adopts far more LS character (Table 2). Specifically the Fe–N bond lengths are seen to decrease from 2.08 to 2.16 Å in the 298 K structure to 1.93–2.02 Å in the 100 K structure. The most important bond angle is N$_{pyr}$–Fe–N$_{triaz}$ as it is a part of the five membered chelate ring formed when the bidentate pocket binds to the iron(II) centre [N(1)–Fe(1)–N(2) in Fig. 4]. This angle increased from 77.2(5)° to 80.3(6)° upon cooling, becoming closer to the pure octahedral angle (90°) as expected for a LS complex.

The **adpt** ligand strands are relatively planar: the angles between the mean plane of the triazole ring and the mean planes of the two, crystallographically independent, attached pyridine rings is less than 5°. Due to coordination to the iron(II) centre, the coordinated pyridine ring is expected to be constrained to be co-planar with the triazole ring. The uncoordinated pyridine ring, however, is free of such constraints and has the potential to rotate about the linking C–C bond, albeit at the cost of reducing the extent of conjugation between them, allowing this ring to adopt a non co-planar arrangement. However, as is frequently observed, the uncoordinated pyridine ring is also very close to co-planar with the rest of the ligand strand, and it is flipped 180° about the C–C bond, i.e. the uncoordinated nitrogen, N(4), is positioned anti to the uncoordinated triazole nitrogen, N(3) (Fig. 4). This anti co-planar arrangement is stabilized by the retention of conjugation, reduction of lone pair repulsions (which would be associated with the syn co-planar configuration), and the intramolecular hydrogen bond that forms between one of the hydrogen atoms on the amino N^4 substituent, N(6), and the uncoordinated pyridine nitrogen, N(4) [N(6)···N(4) = 2.83(2) Å, and ∠N(6)–H(6A)···N(4) = 141(1)°]. This hydrogen bond is present, and identical, at both temperatures studied.

The structure is further stabilized by a second, weaker, hydrogen bond that forms between the second hydrogen atom on the N^4 amino substituent and an uncoordinated cyano nitrogen atom of a TCNQ anion on an adjacent molecule [N(6)···N(9)* = 3.25(2) Å and ∠N(6)–H(6A)···N(9)* = 147(2)°] (HS structure). Unlike the stronger hydrogen bond this one does not remain identical on switching spin states: in the LS structure it is seen to contract [N(6)···N(9)* = 3.14(2) Å and ∠N(6)–H(6A)···N(9)* = 146(2)°], as is expected with a contraction of Fe–N bond lengths.

The TCNQ anion coordinates through only one of is its four cyano groups. [Fe^{II}(**adpt**)$_2$(TCNQ)$_2$] packs in a way such that the TCNQ anions form stacked dimers. On changing from HS to LS the distance between the mean planes of the TCNQ molecules in these stacked dimers reduced from 3.22 to 3.15 Å. This stacking interaction is believed to be critical to the strong pairing of adjacent radical anion spins such that they are not observed.

2.2.2. [Fe^{II}(**adpt**)$_2$(NCX)$_2$] family

Real and co-workers prepared a series of related mononuclear bis complexes (Fig. 2) of **adpt** in which they varied the coordinated anion used [33,42,65]. These complexes have the
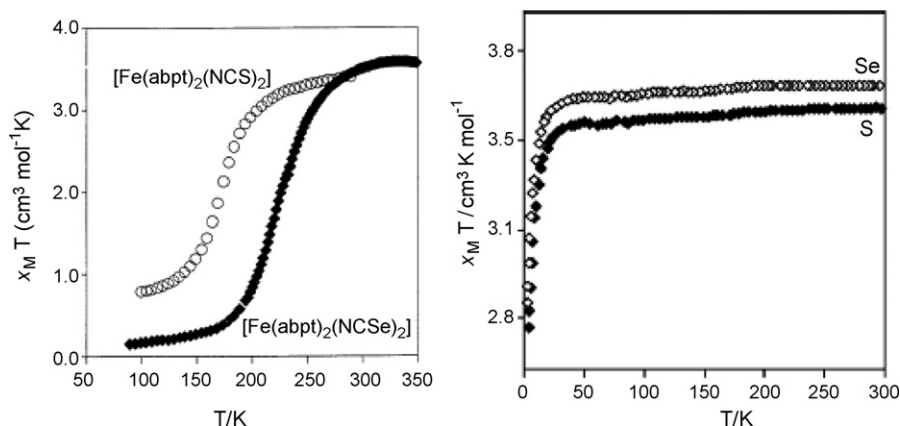
Fig. 5. Variable temperature magnetic data for the red (LHS) and orange (RHS) polymorphs of [Fe^{II}(**adpt**)$_2$(NCS)$_2$] and [Fe^{II}(**adpt**)$_2$(NCSe)$_2$]. (LHS) reprinted with permission from Inorg. Chim. Acta 291 (1999) 279. Copyright 1999, Elsevier. (RHS) reprinted with permission from Monatsh. Chem. 134 (2003) 285. Copyright 2003, Springer Wien.

general formula [Fe^{II}(**adpt**)$_2$(NCX)$_2$] where X = S, Se or NCN (thiocyanate, selenocyanate or dicyanamide). All three complexes were prepared, at room temperature under argon, in a stoichiometric manner.

For the complex where X = S or Se, initially Fe^{II}(ClO$_4$)$_2$.6H$_2$O and KXCN (1:2) were reacted in acetone. The precipitated KClO$_4$ was filtered off leaving an acetone solution of "Fe^{II}(NCX)$_2$" to which was added a methanol solution of two equivalents of **adpt**, resulting immediately in a pink crystalline product.

Interestingly, both [Fe^{II}(**adpt**)$_2$(NCS)$_2$] and [Fe^{II}(**adpt**)$_2$(NCSe)$_2$] crystallized in two polymorphs [43]. X-ray quality (single) crystals of the two polymorphs, red and orange, were obtained by the slow evaporation under a stream of argon of a methanol/dichloromethane (1:1) solution and a water/methanol solution, respectively. This is a clear illustration of the importance solvent choice – despite there being no solvent present in the resulting crystals.

For the dicyanamide complex, i.e. where X = NCN, two equivalents of **adpt** in a methanol solution were added to a water/methanol solution of FeSO$_4$·7H$_2$O (1 equivalent). To

the resulting orange solution was added an aqueous solution of two equivalents of NaN(CN)$_2$. The resulting mixture was filtered and evaporated under an argon stream to yield orange X-ray quality (single) crystals of [Fe^{II}(**adpt**)$_2$(N(CN)$_2$)$_2$], in 50% yield.

For the red polymorphs of X = S and Se, gradual, temperature dependent, SCO events were observed with $T_{1/2}$ values of 180 and 224 K respectively (Fig. 5). In stark contrast to the red polymorphs, the iron(II) centre in the orange polymorphs remains in the HS configuration from 300 to 2 K at ambient pressure (1 bar).

However, when the pressure is increased to 4.4 kbar, an incomplete thermal crossover occurs for the orange polymorph of [Fe^{II}(**adpt**)$_2$(NCSe)$_2$], with $T_{1/2}$ = 65 K (Fig. 6). As the pressure is increased further, to 5.6, 8.6 and 10.5 kbar, complete spin transitions are observed with $T_{1/2}$ values of 106, 152 and 179 K respectively (Fig. 6). In slow cooling and heating modes (0.1 K min^{-1}), i.e. thermodynamic equilibrium conditions, all of these spin transitions display a narrow hysteresis loop of 2 K width. Interestingly there is a linear relationship between the applied pressure and the $T_{1/2}$.
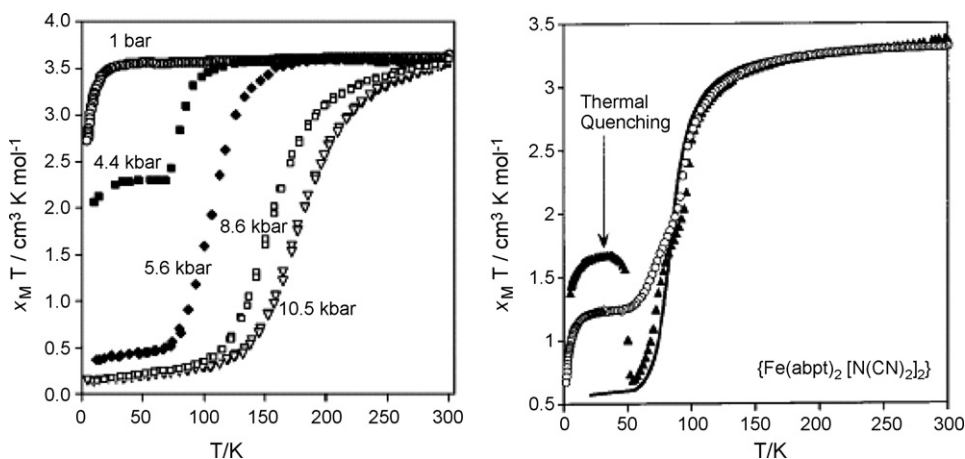
Fig. 6. Variable temperature magnetic data for: (LHS) the orange polymorph of [Fe^{II}(**adpt**)$_2$(NCSe)$_2$] measured under pressures ranging from 1 to 10.5 bar and (RHS) [Fe^{II}(**adpt**)$_2$(N(CN)$_2$)$_2$] (open circles) and thermal quenching results (black triangles). (LHS) reprinted with permission from Monatsh. Chem. 134 (2003) 285. Copyright 2003, Springer Wien. (RHS) reprinted with permission from Inorg. Chem. 40 (2001) 3986. Copyright 2001, American Chemical Society.

In contrast, for the dicyanamide complex, X = NCN, an incomplete SCO event (84 K) that occurred in two steps was observed (Fig. 6; RHS, circles). This SCO event starts from fully HS, has a 'blip' in the middle at ca. 100 K where the gradient of the fitted curve decreases signifying the start of the second step, the second step ends with a plateau at 60–25 K (χT = 1.23 cm^3 mol^{-1} K) which is consistent with an incomplete crossover, with 37% of the sample remaining kinetically trapped in the HS form, despite the 'normal' cooling rates employed. The $T_{1/2}$ of 84 K is one of the lowest SCO transitions recorded, and enabled the kinetic properties of the HS $\rightarrow$ LS conversion to be studied, for example via thermal quenching which showed that on warming the kinetically trapped material above its relaxation temperature it reverted to fully low spin. However, it should be noted that in a brief communication to the Second International Conference on Photo-induced Phase Transitions, Pillet et al. [66] suggested that a second crystal phase, containing two (not one) crystallographically independent molecules in the asymmetric unit, is present in the bulk sample that was used for the initial magnetic measurement by Moliner et al. [33]. Further studies to probe the possible significance and effects of this second phase are underway.

Light Induced Electronic Spin State Trapping (LIESST) was used to further probe the nature of the HS $\rightarrow$ LS conversion in the red polymorphs of X = NCS and NCSe and in the X = NCN complexes (Fig. 7). [Fe^{II}(**adpt**)$_2$(N(CN)$_2$)$_2$] showed a T_{liesst} of 52 K (T_{liesst} is the temperature at which the first derivative of the warming curve reaches a minimum) [42,67]. The red complexes of [Fe^{II}(**adpt**)$_2$(NCS)$_2$] and [Fe^{II}(**adpt**)$_2$(NCSe)$_2$] both displayed interesting and unique LIESST properties. These two complexes were studied in two LIESST modes, using red light. In the first mode light irradiation was excluded in the warming step, while in the second experiment the light irradiation was maintained throughout the warming process. The results were the same in both cases with T_{liesst} values of 40 and 32 K for X = S and Se respectively (Fig. 7, top). However, when maintaining light irradiation with cooling, a new type of hysteresis was observed, Light-Induced Thermal Hysteresis (LITH, Fig. 7, bottom). This effect had previously been reported only twice [68,69]. The effect was attributed to the two operative effects observed under light irradiation, firstly the light induced trapping of the sample in the metastable HS state, and secondly the relaxation from the HS state to the LS ground state.

Single crystal X-ray structures were determined for all five complexes (X = NCN, and both red and orange polymorphs of X = S and Se) at 293 K, a temperature at which all of them are in the HS state (Fig. 8, Tables 1 and 2). All five of them are of the mononuclear bis type (Fig. 2) and are isostructural, but not isomorphous, with the 298 K structure of [Fe^{II}(**adpt**)$_2$(TCNQ)$_2$] described by Haasnoot and co-workers (Fig. 4, Table 1) [61]. Each structure contains two equatorially bound **adpt** ligands and two axially bound (trans) co-ligands, pseudo halide anions [NCS$^-$, NCSe$^-$ or N(CN)$_2$$^-$] in the case of the complexes prepared by Real and coworkers and TCNQ$^-$ in the case of the complex prepared by Haasnoot and co-workers.

Structurally the orange polymorphs are very similar to the red polymorphs, with two equatorially bound **adpt** ligands and
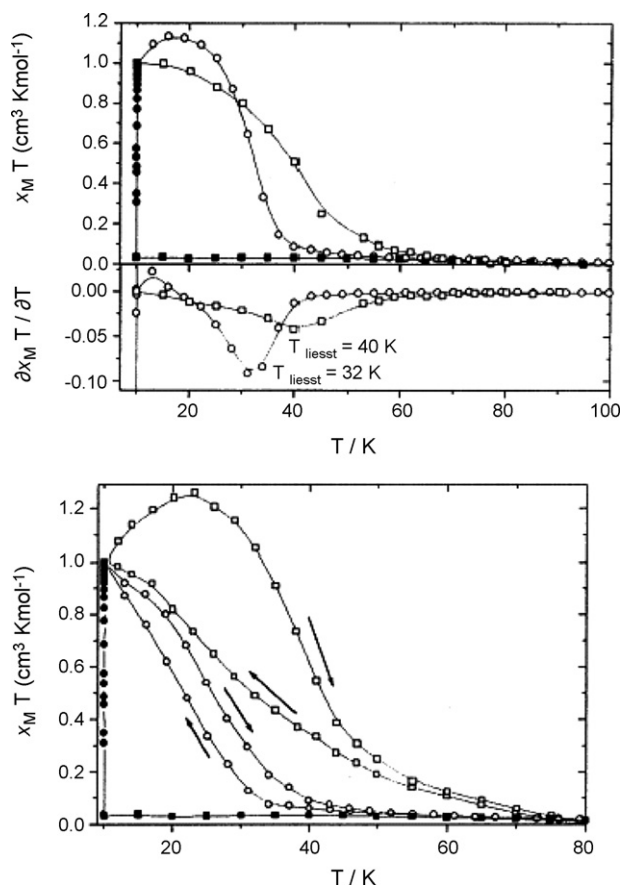

Fig. 7. LIESST experimental results for [Fe^{II}(**adpt**)$_2$(NCS)$_2$] (open squares) and [Fe^{II}(**adpt**)$_2$(NCSe)$_2$] (open circles): Standard LIESST experiment (top) and experiment showing LITH (irradiation in both cooling and warming modes) (bottom). Black squares show cooling without irradiation and black circles the result of irradiating at 10 K for 1 h. Reprinted with permission from Inorg. Chim. Acta 291 (1999) 279. Copyright 1999, Elsevier.

two axially bound NCX (X = S, Se) anions. In the orange polymorphs the Fe—N bond lengths are slightly longer (Table 2), but the major difference is the absence of a hydrogen bond between the uncoordinated pyridine ring and the amino head group. This
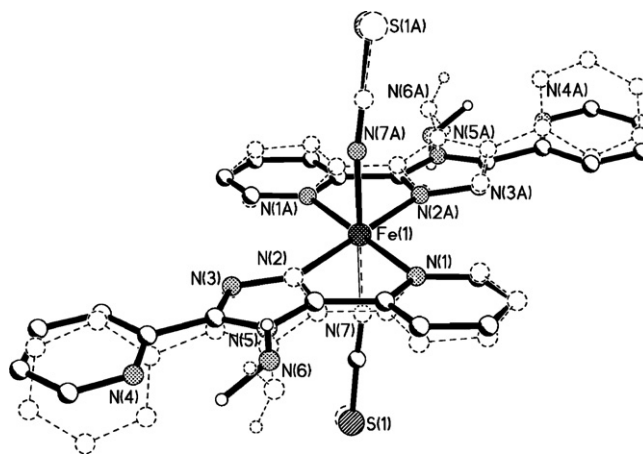

Fig. 8. Superposition of the red (solid lines) and orange (dotted lines) polymorphs of [Fe^{II}(**adpt**)$_2$(NCS)$_2$] at 298 K. At this temperature Fe(1) is HS in both polymorphs. These figures were generated from data obtained from the Cambridge Crystallographic Data Centre as published originally in [42,43].
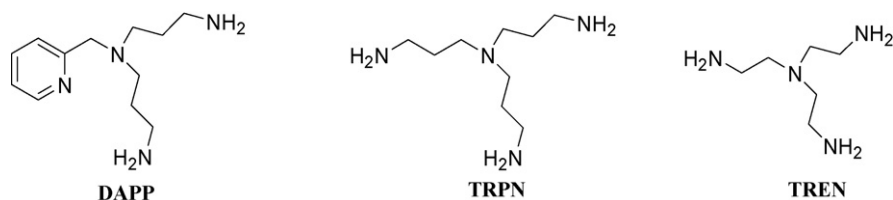
Fig. 9. A selection of tetradentate ligands employed in conjunction with di(2-pyridyl)-triazole ligands. Only one of the DAPP derived complexes has been structurally characterized to date.

results in a much less planar ligand conformation, which in turn alters the packing of the molecules within the unit cell. For the NCS complex the angle between the mean plane of the unco-ordinated pyridine and that of the triazole is $8.31°$ for the red polymorph and $29.85°$ for the orange polymorph (Fig. 8); the analogous angles for the NCSe complex are $7.97°$ and $30.73°$, respectively. The authors proposed that this difference in crystal packing causes the lengthening of the Fe−N bonds in the orange polymorphs relative to the red polymorphs, as the uncoordi-nated and less restrained pyridine ring induces a steric effect on the neighbouring molecule causing a distortion of its octahedral iron(II) centre.

2.2.3. $[Fe^{II}(adpt)(L)]^{2+}$ family

The ligand **adpt** has also been used in conjunction with a tetradentate ligand, DAPP (Fig. 9), to form an iron(II) complex, $[Fe^{II}(adpt)(DAPP)](ClO_4)_2$, where DAPP = [bis(3-aminopropyl)(2-pyridylmethylamine] [34]. This was synthe-sised by adding, under N_2, one equivalent of DAPP in a deoxygenated methanol/ethanol solution to one equivalent of $Fe(ClO_4)_2 \cdot 6H_2O$ (in the same solvent mixture) resulting in the formation of a yellow solution. The addition of half an equivalent of **adpt** (the reaction is non-stoichiometric – this was necessary in order to avoid formation of the tris complex) in methanol gave a red–orange solution. After filtering the solution and leaving it to stand at room temperature overnight yellow–brown crystals of X-ray quality were obtained.

Once again the complex was mononuclear with an octahedral iron(II) ion. But in this case the single **adpt** ligand occupies two of the iron(II) binding sites and DAPP occupies the other four, giving the iron centre an N_6 coordination sphere. This complex displays an abrupt SCO event coupled with thermally dependant hysteresis. On cooling the sample from 295 K, χT remains at 3.55 cm³ mol⁻¹ K ($\mu_{eff} = 5.33\ \mu_B$) until 176 K, where an abrupt and complete transition, which occurs over 10 K, starts. A broad plateau region is observed, with a χT of 0.10 cm³ mol⁻¹ K ($\mu_{eff} = 0.89\ \mu_B$) at 86 K, which is close to the expected value for LS iron(II). On warming the sample it remains in the LS con-figuration until 176 K where another abrupt SCO event occurs, which is complete by 184 K (Fig. 10). Thermally dependent hysteresis is highly desired in SCO complexes. In this case the transition temperatures are $T^{\downarrow}_{1/2} = 171$ K and $T^{\uparrow}_{1/2} = 181$ K and hence the hysteresis width is just 10 K.

^{57}Fe Mössbauer spectroscopy was also used to further exam-ine the nature of the SCO event detailed above (Fig. 11). The study was carried out over the temperature range 80–293 K in both heating and cooling modes. In the spectrum obtained at

Fig. 10. Thermal hysteresis loop observed in the variable temperature magnetic data for $[Fe^{II}(adpt)(DAPP)](ClO_4)_2$. $T^{\downarrow}_{1/2} = 171$ K and $T^{\uparrow}_{1/2} = 181$ K. Reprinted with permission from Inorg. Chem. 43 (2004) 227. Copyright 2004, American Chemical Society.

211 K there is a distinctly HS iron(II) centre, which remains HS when cooling to ∼180 K where it begins to disappear giving a spectrum characteristic of LS iron(II). At temperatures below 170 K in both cooling and warming modes the spectra are charac-teristic for that of LS iron(II). In the warming mode the spectrum at 185 K was found to be different to that observed in the cool-ing mode, in this instance the spectrum was characteristic of LS iron(II), thus confirming the occurrence of hysteresis.

The higher temperature Mössbauer measurements (211 K) showed that spectral dissymmetry was present with little broad-ening of the lines. There are two possible reasons for this

Fig. 11. Mössbauer spectra of $[Fe^{II}(adpt)(DAPP)](ClO_4)_2$ at a range of different temperatures. Reprinted with permission from Inorg. Chem. 43 (2004) 227. Copyright 2004, American Chemical Society.

Fig. 12. Structure of [Fe^{II}(**adpt**)(DAPP)](ClO₄)₂ at 123 K (solid lines) fitted to those obtained at 293 and 183 K 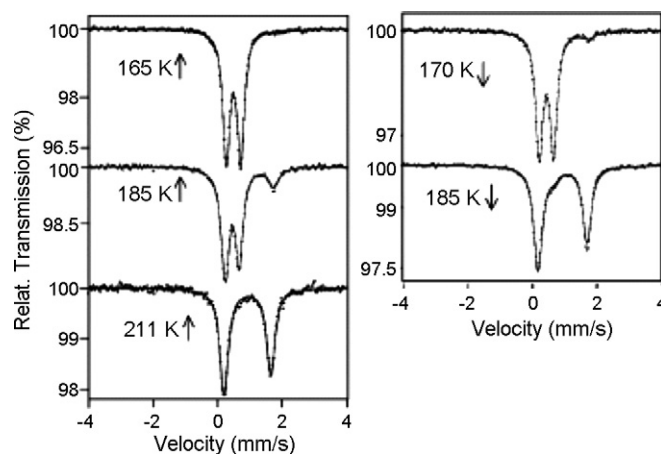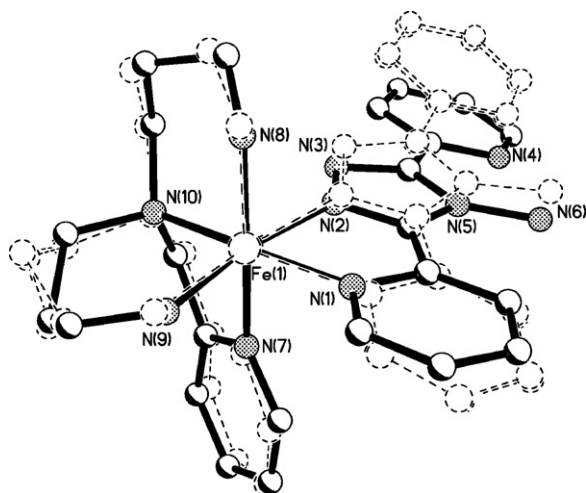(both in dotted lines; cation structure almost identical at these two temperatures – see text). This figure was generated from data obtained from the Cambridge Crystallographic Data Centre as published originally in [34].

observation, a texture effect in the sample or fast relaxation between two crystallography similar configurations (relaxation rates $\gtrsim 10^8\,\text{s}^{-1}$). To probe this effect spectra were obtained at 200 K in two different orientations, Z-axis relative to the γ-ray source direction, of the sample [$(Z \parallel \gamma)$ and $(Z, \gamma = 40°)$]. The spectra were both very similar thus emphasizing the fast relaxation effect, hence two HS species are most likely present, which are suggested to be due to the DAPP ligand adopting two different conformations.

The X-ray crystal structure of this complex was measured at three different temperatures (Figs. 12 and 13; Tables 1 and 3): well before the SCO event (293 K), within the hysteresis loop (cooled to 183 K) and after all SCO has occurred (123 K).

The structures at all three temperatures are in the monoclinic centrosymmetric $P2_1/n$ space group (Table 1). The structure determinations reveal an iron(II) centre with an N₆ coordination geometry containing one **adpt** binding in a bidentate fashion, and the remaining four coordination sites occupied by the DAPP ligand strand (one pyridine and three aliphatic nitrogen donors). The use of DAPP leads to the possibility of either a facial or meridional configuration. The complex adopts the *fac* arrangement, which is chiral, and the unit cell (Z = 4)

Fig. 13. Hydrogen bonding interactions seen in the structure of [Fe^{II}(**adpt**)(DAPP)](ClO₄)₂ (top = 293 K, bottom = 123 K). For a full list of hydrogen bond lengths and angles as well as symmetry operations see the original reference [34].

contains two pairs of symmetry related left and right handed enantiomers.

The structure obtained at 293 K shows bond lengths [2.167(3)–2.233(3) Å] and angles which are characteristic for HS iron(II) (Table 3). The bond lengths between the iron(II) centre and **adpt** are similar to those observed in the previous HS structures (Table 2), including the common observation that the $N_{pyridine}$–Fe bond is longer than the $N_{triazole}$–Fe bond. The *cis* N–Fe–N bond angles range from 74.2(2)° to 97.0(2)°, with the largest deviation from 90° seen in the five membered

Table 3
Bond lengths and angles for [Fe^{II}(**adpt**)(DAPP)](ClO₄)₂ at three different temperatures

Bond lengths (Å) and angles (°)	[Fe(**L**)(DAPP)] 293 K	[Fe(**L**)(DAPP)] 183 K	[Fe(**L**)(DAPP)] 123 K
Fe–N$_P$	2.252(3)	2.223(5)	2.028(3)
Fe–N$_T$	2.184(3)	2.158(4)	1.983(3)
Fe–N$_7$	2.179(4)	2.158(5)	1.977(3)
Fe–N$_8$	2.167(3)	2.151(5)	2.040(4)
Fe–N$_9$	2.233(3)	2.206(5)	2.077(3)
Fe–N$_{10}$	2.178(4)	2.162(5)	2.027(3)
Cis N–Fe–N range	74.2(2)–97.0(2)	74.9(2)–96.4(2)	80.5(1)–94.8(1)
Trans N–Fe–N range	163.2(2)–171.8(2)	163.9(2)–173.2(2)	169.7(1)–177.4(1)
Cis N$_T$–Fe–N$_P$	74.2(2)	74.9(2)	80.5(1)

chelate rings, as the six membered chelate rings are more flexible and hence more accommodating of closer to pure octahedral angles. Most previous iron(II) structures involving **adpt** feature a hydrogen bond between the amino N^4 substituent and the uncoordinated pyridine ring, and this is observed in this structure too. The structure contains two six membered chelate rings due to the coordination of DAPP. One of these rings adopts a chair conformation, while the other forms a disordered half-boat conformation, where one of the carbon atoms is disordered over two sites (0.5:0.5). A second disorder is present, involving a perchlorate anion, Cl(2), which is disordered over two sites (0.5:0.5). The relevance of these disorders is discussed later.

The packing of the molecules within the unit cell in this complex is an important consideration as the observation of hysteresis indicates that there is cooperativity present between individual molecules. At 293 K there is a strong hydrogen bonding network observed. Each individual molecule forms 13 hydrogen-bonds (five intramolecular and eight intermolecular), 4 of which involve amine nitrogen atoms bound directly to the iron(II) centre (Fig. 13), and two types of π–π interactions, resulting in a strongly connected network of molecules.

In the cooling mode structure (183 K) the overall geometry of the iron(II) centre is very similar to that at 293 K and the overall conformations of the two ligands are also the same at both temperatures (Fig. 13). The disorder in the half-boat conformation portion of the DAPP ligand remains, however, the C(21A) position is now preferred (0.7:0.3). The Cl(2) perchlorate anion is no longer disordered as it has undergone an order–disorder transition on cooling. The packing at 183 K remains identical to that observed at 293 K, with only a slight variation in cell parameters [an overall decrease of 2.0% (60 Å^3)]. The intermolecular interactions (hydrogen-bonding and π–π stacking) are shorter, consistent with a strengthening of intermolecular interactions on cooling.

The low temperature structure (123 K) reveals some major differences to the previous two temperatures (Table 3, Fig. 13). The geometry of the iron(II) centre has altered such that it is now characteristic of LS iron(II): the bond lengths are all shortened by ~0.2 Å and the bond angles are closer to a pure octahedral arrangement. Another important change is that at this temperature the C(21) methylene carbon in the half-boat configuration is no longer disordered. This indicates that a second disorder–order transition occurs on cooling low enough to switch from HS to LS. The initially disordered perchlorate anion (in the 293 K) structure is now a well behaved anion, further increasing the order within the crystal lattice. The volume of the unit cell decreased further, as expected for a transition from the larger HS iron(II) to the smaller LS form. However the significant reduction in volume [5.15%, 158.4 Å^3 from 3074(1) Å^3 at 293 K to 2915.3(3) Å^3 at 123 K] is not only associated with the shortening of the Fe–N bonds, but also a thermal contraction of the lattice which has occurred thanks to a change in the intermolecular network. The pattern of hydrogen bonds has changed and the total number of them has increased (Fig. 13). The two types of π–π-stacking are still observed, however the type in the c direction is different as there are fewer C$\cdots$C contacts.

This study provides a good illustration of the role intermolecular interactions play in generating samples which exhibit hysteresis. The structures obtained in the HS and LS states show a change in intermolecular interactions is accompanied with the spin state transition, and reinforces the idea that cooperativity plays an important role in hysteresis [70]. The order–disorder transitions seen in this complex are of considerable interest as disorder is seen to disappear on conversion to the LS structure. The group also examined the effect that the counter anion plays on the magnetic properties. Although not structurally characterized, the group prepared analogous complexes where the anion is BF_4^- and PF_6^- instead of ClO_4^-. The magnetic properties of the BF_4^- analogue are similar to those of the ClO_4^- complex, with a hysteresis loop centred around a slightly higher temperature. Contrasting with this, the PF_6^- complex displays a gradual SCO without hysteresis, at lower temperatures as expected based on the size of this counter anion [71].

Complexes similar to those mentioned above, $[Fe^{II}(\textbf{adpt})(L)]^{2+}$, have also been prepared with L = TRPN or TREN (Fig. 9) [28,45]. These, however, have not been characterized by means of single crystal X-ray diffraction.

The complexes were prepared by the addition of one equivalent of L (TRPN or TREN, in methanol) to one equivalent of $[Fe^{II}(OH_2)_6]X_2$ (X = ClO_4^- and NO_3^- respectively, in methanol) followed by one equivalent of **adpt** (in acetonitrile/water 3:1) at 60 °C. The solution was stirred at RT for 4–6 h then allowed to stand for 6 days resulting in brown microcrystalline complexes of $[Fe^{II}(\textbf{adpt})(TRPN)](ClO_4)_2$ and $[Fe^{II}(\textbf{adpt})(TREN)](NO_3)_2(H_2O)_2$ in 50% and 55% yields respectively. Without crystal structures a definitive statement that the two ligands have coordinated generating an N_6 Fe(II) centre cannot be made, however it can be strongly inferred from sporting methods including the analysis of the IR and electronic spectra.

The effective magnetic moment of the TREN complex at 298 K was 5.43 B.M., indicating a HS Fe(II) centre. In the case of the TRPN complex a variable temperature measurement was carried out: at 298 K an effective magnetic moment of 5.45 B.M., characteristic of HS Fe(II) was observed, while at 80 K the magnetic moment was 3.22 B.M., characteristic of the presence of some LS Fe(II). Strangely, further details were not provided.

2.3. Complexes of m/p-methylphenyl-3,5-di(2-pyridyl)-1,2,4-triazole (*m/p*-mdpt)

Only one study to date has been carried out on an N^4-substituted 3,5-di(2-pyridyl)-triazole ligand that was not **adpt**. The ligands used in that study contain N^4 tolyl substituents (*p*-tolyl and *m*-tolyl, Fig. 1) [*m*-**mdpt** and *p*-**mdpt** i.e. *m/p*-methylphenyl-3,5-di(2-pyridyl)-1,2,4-triazole] [44]. The iron(II) complexes of these ligands, $[Fe^{II}(\textbf{\textit{m/p}-mdpt})_2(NCS)_2]$, are both of the mononuclear bis type, containing two NCS$^-$ anions to complete the octahedral coordination sphere and achieve charge balance [30]. Both complexes were prepared in the following way. Under argon to a solution of KSCN (2 equivalents) in anhydrous methanol was added a solution of FeSO$_4\cdot$7H$_2$O (1 equivalent) in methanol. After stirring

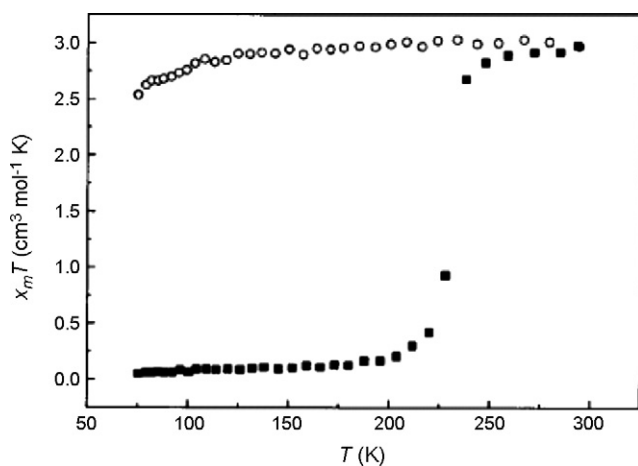Fig. 14. Plots of χT as a function of temperature for [Fe^{II}(**p-mdpt**)$_2$(NCS)$_2$] (solid squares) and [Fe^{II}(**m-mdpt**)$_2$(NCS)$_2$] (hollow circles). Reprinted with permission from Chem. Mater. 14 (2002) 838. Copyright 2002, American Chemical Society.

for 15 min at room temperature the mixture was filtered and the K$_2$SO$_4$ precipitate washed with anhydrous methanol. The methanol fractions, containing "Fe(SCN)$_2$", were added dropwise to a methanol solution of the appropriate ligand (2 equivalents) resulting in the immediate formation of a microcrystalline product. Washing with water and drying under an argon stream gave the desired products of [Fe^{II}(**p-mdpt**)$_2$(NCS)$_2$] and [Fe^{II}(**m-mdpt**)$_2$(NCS)$_2$] as a red–brown solid (91%) and a red solid (85%) respectively.

The magnetic profiles of the two complexes are vastly different (Fig. 14). Over the temperature range 75–300 K [Fe^{II}(**p-mdpt**)$_2$(NCS)$_2$] was seen to have an abrupt thermally dependant SCO event with $T_{1/2} = 231$ K. In contrast, [Fe^{II}(**m-mdpt**)$_2$(NCS)$_2$] displays no SCO and the iron(II) centre remains in the HS configuration at all temperatures studied. The arrangement of ligands around the iron(II) plays a pivotal role in this different behaviour and will be discussed later.

To further probe the SCO event observed for [Fe^{II}(**p-mdpt**)$_2$(NCS)$_2$], variable temperature EXAFS and IR were employed (Fig. 15). As anticipated, the EXAFS spectra recorded

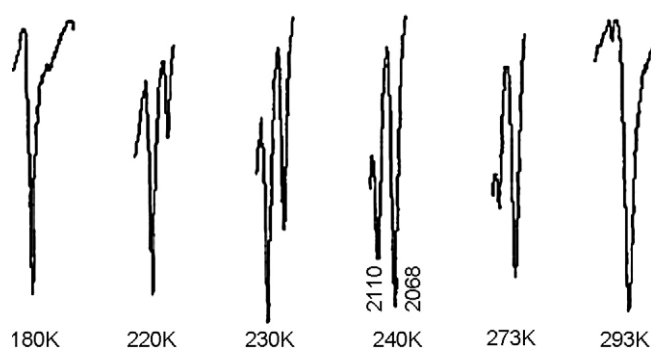Fig. 15. Infrared absorptions of the NCS$^-$ anions in [Fe^{II}(**p-mdpt**)$_2$(NCS)$_2$] as a function of temperature. Reprinted with permission from Chem. Mater. 14 (2002) 838. Copyright 2002, American Chemical Society.

on either side of the $T_{1/2}$ value show a decrease of $\sim$0.2 Å for the Fe–N bond lengths. Variable temperature IR spectroscopy (Fig. 15) was used to monitor the SCO event by monitoring the C≡N stretching vibration of the NCS group. IR spectroscopy also allows one to differentiate between *cis*- and *trans*- bound bis-thiocyanates, as a *cis* arrangement has a splitting of the C≡N peaks, while a *trans* arrangement does not and results in singlet peaks [72,73]. The singlets observed at $\approx$2068 and $\approx$2110 cm^{-1} for the HS and LS structures respectively indicated a *trans* arrangement of NCS$^-$ molecules. On cooling from 293 K the LS singlet peak at $\approx$2110 cm^{-1} increases in intensity to a point where it becomes the dominant C≡N feature [$\sim$230 K ($\sim$$T_{1/2}$)]. By 180 K the HS singlet peak ($\approx$2068 cm^{-1}) is completely gone and only the LS singlet peak at $\approx$2110 cm^{-1} peak remains.

The X-ray crystal structures of these two complexes at 293 K, at which both complexes are expected to be HS, reveal that the ligand binding pattern about the iron(II) centres differ: a *trans* NCS configuration is observed for [Fe^{II}(**p-mdpt**)$_2$(NCS)$_2$] and a *cis* NCS configuration for [Fe^{II}(**m-mdpt**)$_2$(NCS)$_2$] (Fig. 16, Table 4).

The complex [Fe^{II}(**p-mdpt**)$_2$(NCS)$_2$] crystallizes in the triclinic centric *P*-1 space group. It displays a very similar structure to that of [Fe^{II}(**adpt**)$_2$(NCS)$_2$], in that the iron(II) is on a centre of inversion, and that it contains two NCS molecules in a *trans*

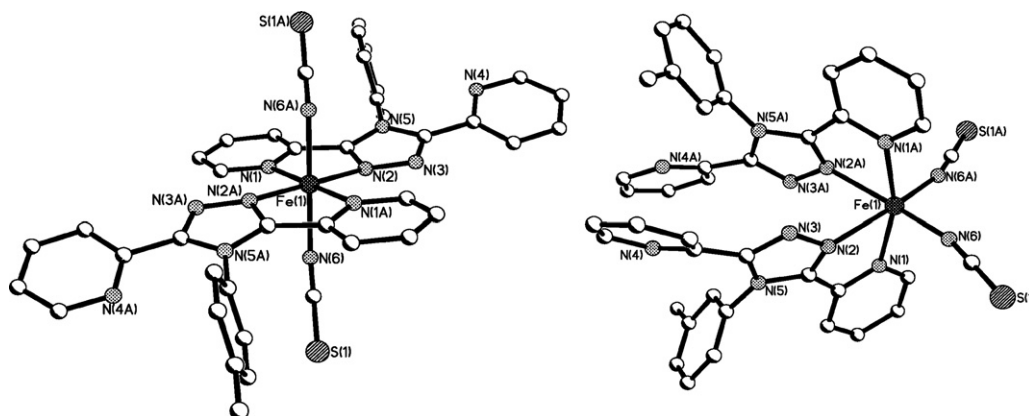Fig. 16. Structures of (LHS) [Fe^{II}(**p-mdpt**)$_2$(NCS)$_2$] and (RHS) [Fe^{II}(**m-mdpt**)$_2$(NCS)$_2$], at 293 K. These figures were generated from data obtained from the Cambridge Crystallographic Data Centre as published originally in [30].

Table 4
Bond length and angle data for [Fe^{II}(**p-mdpt**)$_2$(NCS)$_2$] and [Fe^{II}(**m-mdpt**)$_2$(NCS)$_2$] at 293 K

Bond lengths (Å) and angles (°)	[Fe(**p-mdpt**)$_2$(NCS)$_2$] 293 K	Bond lengths (Å) and angles (°)	[Fe(**m-mdpt**)$_2$(NCS)$_2$] 293 K
Fe–N$_P$	2.213(3)	Fe–N$_P$	2.217(2)
Fe–N$_T$	2.192(2)	Fe–N$_T$	2.248(3)
Fe–N$_X$	2.114(3)	Fe–N$_X$	2.051(3)
N$_T$–Fe–N$_P$	74.17(10)	N$_T$–Fe–N$_P$	73.03(9)
N$_T$–Fe–N$_P$*	105.83	N$_T$–Fe–N$_T$‡	75.72(15)
N$_T$–Fe–N$_X$	94.52(11)	N$_T$–Fe–N$_X$	92.66(12)
N$_T$*–Fe–N$_X$	85.49	N$_P$–Fe–N$_P$‡	163.24(13)
N$_X$–Fe–N$_P$	95.30(12)	N$_X$–Fe–N$_P$	97.34(9)
N$_X$–Fe–N$_P$*	84.70	N$_X$–Fe–N$_X$‡	102.13(18)
Fe–N$_X$–C$_X$	148.3(3)	Fe–N$_X$–C$_X$	164.5(3)

Symmetry operations to generate equivalent atoms: (*) −*x*, −*y*, −*z*; (‡) −*x*, *y*, 0.5 − *z*.

arrangement (consistent with the IR data), and two equatorial di(2-pyridyl)-triazole ligand molecules (Fig. 16, LHS).

Once again the Fe–N bond lengths, 2.114(3) to 2.213(3) Å, are characteristic of HS iron(II) and are similar to those seen previously, with Fe–N$_{triazole}$ being considerably shorter than Fe–N$_{pyridine}$. The *cis*-N–Fe–N angles are also consistent with HS iron(II), ranging widely, from 74.17(10)° to 95.30(12)°.

Unlike the previous NCX structures of **adpt** [Table 2, overall min ∠Fe–N$_X$–C$_X$ = 151(1)° is for the TCNQ structure at 298 K; min ∠Fe–N$_X$–C$_X$ for X = S is 169.7(1)° for red polymorph at 293 K], the NCS anions are bound to the iron at a greater angle, ∠Fe–N$_X$–C$_X$ = 148.3(3)°, in this complex of **p-mdpt**. The ligand strands in this complex are, in comparison to those in the **adpt** complexes, relatively nonplanar: the angles formed between the pyridine rings and the central triazole ring are ∠Py$_{coord}$–Triazole = 11.6(3)° and Py$_{uncoord}$–Triazole = 14.8(3)°. This is understandable considering the lack of a hydrogen bonding group positioned off N^4 to constrain the uncoordinated ring. The *p*-tolyl moiety is twisted at near right angles (82.86°) to the central triazole ring, minimizing any π mediated electron donation from the *p*-tolyl group. The packing of the complex within the cell involves π–π stacking between the uncoordinated pyridine rings, which stabilizes the extended structure.

The structure of the second complex, [Fe^{II}(**m-mdpt**)$_2$(NCS)$_2$], is very different to that of [Fe^{II}(**p-mdpt**)$_2$(NCS)$_2$]. The complex crystallizes in the monoclinic *C*2/*c* space group and unlike all related complexes the co-ligands are in a *cis* arrangement (Fig. 16).

The Fe–N bond lengths are consistent with that of HS iron(II) as expected from the magnetic profile (Table 4). However this time the Fe–N$_{triazole}$ bond lengths are longer than the Fe–N$_{pyridine}$ bond lengths, in contrast to all of the other structures. This is probably due to the different, more sterically demanding, *cis* binding mode of the **m-mdpt** ligands. The methyl carbon of the *m*-tolyl group is disordered over the two possible sites (with occupancies of 0.73 and 0.27). Packing in this cell is based on van der Waals interactions. This subtle change in the N^4 substituent of the ligand from *p*- to *m*-tolyl has had dramatic consequences with the formation of a completely different isomer with totally different magnetic properties.

2.4. Comparisons and concluding remarks

The use of these N^4-*substituted* di(2-pyridyl)-1,2,4-triazole-based ligands has facilitated the synthesis of 9 (Table 2) magnetically interesting, structurally characterized, complexes of iron(II), and none of iron(III). These complexes are all mononuclear. They are interesting as they demonstrate that a range of subtle and not-so-subtle changes to the complex can modify the magnetic properties, dramatically in some cases.

A key feature of these N^4-substituted triazole ligands is the possibility of varying the N^4 group [10]. Despite this possibility, to date only complexes containing the commercially available **adpt** or the pair of very closely related synthesised ligands **p-mdpt** and **m-mdpt** have been reported. The effect that changing the N^4 substituent can have is particularly nicely illustrated by the comparison of the three complexes [Fe^{II}(**adpt**)$_2$(NCS)$_2$], [Fe^{II}(**p-mdpt**)$_2$(NCS)$_2$] and [Fe^{II}(**m-mdpt**)$_2$(NCS)$_2$]. The first two complexes are isostructural and the NCS⁻ anions are in a *trans* configuration, while in the third complex the NCS⁻ anions are in a *cis* configuration. Both **p-mdpt** and **m-mdpt** feature a phenyl substituent at N^4 and they differ only in the position of the methyl group on this phenyl ring. This subtle change, from *para* to *meta* positioning of the methyl group, alters the way in which the ligands bind to the iron centre, quite possibly due to the methyl group preventing the formation of layers of molecules when it is in the at the *meta* position as is the case of the *trans* complexes rather favouring the less sterically demanding packing scheme seen for the *cis* arrangement. The magnetic properties of the complexes dramatically change when the N^4-substituent is altered. [Fe^{II}(**adpt**)$_2$(NCS)$_2$] and [Fe^{II}(**p-mdpt**)$_2$(NCS)$_2$] both display temperature dependant SCO events with $T_{1/2}$ values of 180 K and 231 K respectively, thus changing the substituent has shifted the transition temperature substantially. The *cis* complex [Fe^{II}(**m-mdpt**)$_2$(NCS)$_2$] does not display an SCO event and remains in the HS configuration at all temperatures studied, emphasizing the effect that a different isomeric form has, which was in turn influenced by the N^4-substituent.

Other subtle changes to the complex or the preparative route to obtaining the complex also influence the properties of the resulting complex. The formation of red and orange polymorphs of a pair of complexes, simply by varying the solvent used, even

though there is no solvent in the product, must be carefully noted as this had dramatic consequences magnetically.

Perhaps the biggest alteration carried out in the literature has been changing the axial co-ligands, i.e. comparing TCNQ⁻ versus NCS⁻ versus NCSe⁻ versus N(CN)$_2$⁻, as this too resulted in dramatic changes in the magnetic properties of the resulting complexes. The order of $T_{1/2}$ for these counter anions (from highest to lowest) is TCNQ⁻ > NCSe⁻ > NCS⁻ > N(CN)$_2$⁻ corresponding to $T_{1/2}$ values of 280, 224, 180 and 87 K respectively.

While the TCNQ⁻ co-ligand/counter ion has on one occasion given SCO in an iron(II) complex (see above), the NCS⁻, NCSe⁻ and N(CN)$_2$⁻ axial co-ligands/counter anions are well known to often give SCO in iron(II) complexes when they make up part of the N$_6$ coordination sphere. However these ligands do not need to be present to induce SCO in complexes containing 3,5-di(2-pyridyl)-1,2,4-triazole-based ligands. This is exemplified by the iron(II) complex containing **adpt** [occupying only two of the six coordination sites about the iron(II) centre] and also the tetradentate ligand DAPP (Figs. 12 and 13). This complex not only showed an SCO event, but also a hysteresis loop of 10 K. A study into analogous complexes, using the tetradentate ligands TREN and TRPN has been carried out however, despite tantalising room temperature versus 80 K magnetic moments, a full magnetic study has not yet been reported.

The use of these neutral triazole ligands has led exclusively to mononuclear complexes of iron to date. Mostly the reactions were performed in Fe:L 1:2 ratio so such complexes were anticipated, however, in one case it was reported that the same products were also formed from 2:2 reactions which were carried out in an attempt to prepare dinuclear complexes [34]. Dinuclear complexes are expected to be magnetically interesting for a range of reasons, including the possibility of multi-state switching and of interdependence of exchange coupling and SCO, so the general lack of information regarding whether or not attempts (successful or otherwise) to prepare them have been made is disappointing. There are many possible reasons that preparing [Fe$_2^{II}$L$_2$(NCX)$_4$] complexes (L = di(2-pyridyl)-triazole ligand; X = S, Se, NCN etc) may be a very real challenge, including a lack of electron density on the ligand tending to disfavour binding of a second metal ion and hence the isolation of dinuclear products. However, one would expect that if the electron-rich **adpt** (amino group at N^4 should feed lots of electron density in to the triazole ring) were employed in M:L reactions of 2:2 ratio that it should be possible to produce dimetallic products if other factors such as solvent choice etc are carefully chosen. While one strongly suspects that such experiments must have been attempted, if so this was presumably without success as they have not been reported. This represents something of a 'gap' in this literature.

Finally, it is remarkable that only 3 di(2-pyridyl)-triazole ligands, **adpt**, **p-mdpt** and **m-mdpt**, have been used with iron(II) to date, given that 34 ligands of this type, with differing N^4-substituents, are known (Fig S1, ESI). This research group is currently exploring these and other binding modes of di(2-pyridyl)-1,2,4-triazoles, as well as what effect the N^4 substituent has on the magnetic properties of the iron complexes.

3. N^4-unsubstituted-3,5-di(2-pyridyl)-1,2,4-triazole/triazolate ligands

3.1. Introductory remarks

Another variation within this family of di(2-pyridyl)-triazole-based ligands is the N^4-unsubstituted, neutral 3,5-di(2-pyridyl)-1,2,4-triazole ligand (**Hdpt**) and the corresponding anion, the 3,5-di(2-pyridyl)-1,2,4-triazolate ligand (**dpt**⁻) (Figs. 1 and 17). There are four structurally characterized iron complexes containing this ligand type. In stark contrast to the exclusive formation of mononuclear iron(II) complexes with the neutral N^4-substituted triazole ligands (Section 2), the use of the neutral N^4-unsubstituted triazole ligand **Hdpt** facilitated the isolation of a *mononuclear iron*(III) complex (Section 3.2) and even more interestingly the use of the corresponding triazolate ligand **dpt**⁻ facilitated the isolation of *dinuclear* complexes of *both iron*(II) *and iron*(III).

3.2. Complexes of neutral 3,5-di(2-pyridyl)-1,2,4-tria<u>zole</u> (**Hdpt**)

The first such complexes were produced by Tong et al. [46]. They prepared both mononuclear and dinuclear complexes via hydrothermal synthesis starting with iron(III). The first structurally characterized mononuclear iron complex was very interesting as it contained a protonated form of the ligand, **Hdpt** (3,5-di(2-pyridyl)-1,2,4-tria<u>zole</u>), unseen in previous coordination complexes (**III**, Fig. 17). There are three possible forms for **Hdpt** in terms of the position of the acidic proton (Fig. 17), and this is the first structure of any metal complex to contain any neutral form of the ligand.

3.2.1. [Fe^{III}(Hdpt)Cl$_3$(H$_2$O)]·H$_2$O

The complex, [Fe^{III}(**Hdpt**)Cl$_3$(H$_2$O)]·H$_2$O, was prepared by combining a non-stoichiometric 6:1 ratio of FeCl$_3$·6H$_2$O and **Hdpt** in methanol in a Teflon-lined stainless steel autoclave, before sealing and heating to 120 °C for 72 h. Cooling to room temperature and standing for 15 days gave red crystals in 54% yield. The magnetic susceptibility of the complex was seen to be consistent with a 5/2 iron(III) (HS) centre
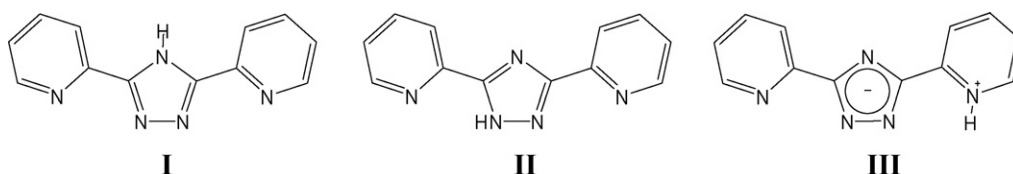

Fig. 17. Three forms of the N^4-unsubstituted, neutral 3,5-di(2-pyridyl)-1,2,4-triazole ligand (**Hdpt**).
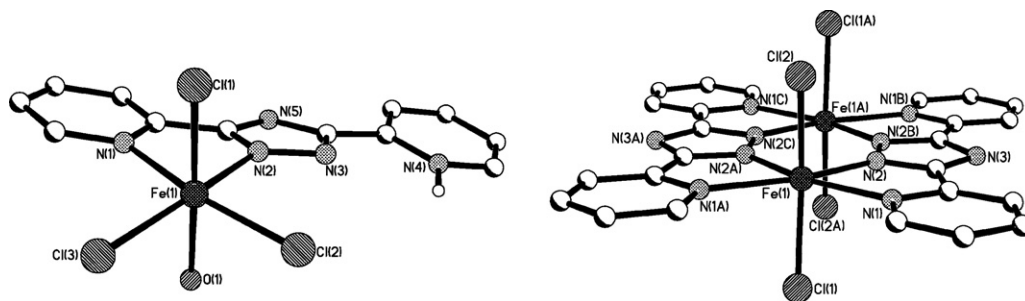
Fig. 18. Structure of the two iron(III) complexes [Fe^{III}(**Hdpt**)Cl$_3$(H$_2$O)]·H$_2$O at 293 K (LHS) and [Fe$^{III}_2$(**dpt**$^-$)$_2$Cl$_4$] at 293 K (RHS). These figures were generated from data obtained from the Cambridge Crystallographic Data Centre as published originally in [46].

at all temperatures studied (2–300 K) as it remained constant with $\chi T = 2.5\ cm^3\ mol^{-1}\ K$ and obeyed the Curie–Weiss law [$\chi_M = C/(T - \theta)$].

The single crystal X-ray structure determination at 293 K revealed a very interesting binding mode (Fig. 18, Table 5). The structure was not a mononuclear bis like the previous triazole complexes. Rather, it contained one ligand strand and one metal ion, where **Hdpt** occupied two binding sites around the iron(III) centre and three chlorides and one water co-ligand completed the remainder of the distorted N$_2$Cl$_3$O octahedral geometry.

As seen in the other mononuclear complexes, the Fe–N$_{pyridyl}$ bond length is again longer than the Fe–N$_{triazolate}$ with distances of 2.226(2) and 2.111(2) Å respectively. The Fe–Cl distances are in the range of 2.2785(7)–2.2999(8) Å, while the Fe–O bond is 2.150(2) Å. These Fe–X bond lengths, and the wide ranging *cis*-X–Fe–X angles, are consistent with the presence of HS Fe(III) as determined from the magnetic moment study.

Interestingly the **Hdpt** ligand is trapped in a zwitterionic arrangement, where the uncoordinated pyridine ring is protonated and the triazole ring is deprotonated, an unprecedented form (Fig. 18, LHS). The hydrogen on the pyridine ring was found from the difference map, and the nitrogen atom distinguished from the carbon atom by the fact that the nitrogen atom is 2.893(3) Å from the oxygen atom, O(1) in the water of crystallization, which is consistent with the presence of a hydrogen bond. The two hydrogen atoms on O(1) were located from difference maps. All of these observations are consistent with the triazole ring being deprotonated and the pyridine ring protonated, to give a neutral **Hdpt**, with an appropriate charge balance for the iron(III) centre being provided by the three chloride ions.

Table 5
Selected bond lengths and angles for [Fe^{III}(**Hdpt**)Cl$_3$(H$_2$O)]·H$_2$O at 293 K

Bond lengths (Å) and angles (°)	[Fe^{III}(**Hdpt**)Cl$_3$(H$_2$O)]·H$_2$O
Fe–N$_P$	2.226(2)
Fe–N$_T$	2.111(2)
Fe–Cl$_1$	2.3002(8)
Fe–Cl$_2$	2.2902(7)
Fe–Cl$_3$	2.2784(7)
Fe–O$_1$	2.148(2)
Cis-angles	73.73(7)–100.86(3)
Trans-angles	162.36(5)–174.51(5)
Cis-N$_P$–Fe–N$_T$	73.73(7)

The complex dimerises via complementary hydrogen bonds between the bound water on one molecule and the N(4) nitrogen on another molecule [O1$_w$···N(4)* = 2.811(2) Å, O1$_w$–H$_{wa}$···N(4)* = 177(3)°]. These dimeric units are part of a 2D network formed by multiple O–H···O, O–H···N, N–H···O, O–H···Cl and C–H···Cl (weak) hydrogen bonds. Offset π–π stacking between pyridyl rings is also present [pyridyl–pyridyl separation of 3.298–3.489 Å and dihedral angle of 4.6(4)°].

3.3. Complexes of deprotonated 3,5-di(2-pyridyl)-1,2,4-tri<u>azolate</u> (**dpt**$^-$)

As mentioned above, the use of **dpt**$^-$ has also facilitated access to the first structurally characterized *dinuclear* complexes with iron(II) or iron(III). These are of great interest due to the possibility of multistep crossovers (HS–HS↔HS–LS↔LS–LS) and exchange-coupling between the iron centers [13,74]. The first dinuclear di(2-pyridyl)–triazolate complexes of iron were prepared by Tong et al. and comprised one di-iron(III) and one di-iron(II) complex, both of which are dinuclear bis complexes (Figs. 18 and 19) [46].

3.3.1. [Fe$^{III}_2$(**dpt**$^-$)$_2$Cl$_4$]

The iron(III) complex [Fe$^{III}_2$(**dpt**$^-$)$_2$Cl$_4$] was prepared in a similar way to the above mononuclear complex (with a 6:1 Fe:**Hdpt** stoichiometry) only instead of methanol as the solvent, acetonitrile was employed, giving purple {rather than the red [Fe^{III}(**Hdpt**)Cl$_3$(H$_2$O)]·H$_2$O} crystals in 82% yield. This subtle change resulted in a vastly different binding mode, i.e. a dinuclear bis complex rather than a simple mononuclear complex. This complex remained in a [HS–HS] (both Fe(III) with $S = 5/2$) configuration at all temperatures studied (2.0–300 K), with a magnetic susceptibility of 8.16 cm^3 mol^{-1} K ($\mu_{eff} = 8.02\ \mu_B$), characteristic of two 5/2 iron(III) centers. The iron(III) centers are weakly antiferromagnetically coupled with $J = -1.65\ cm^{-1}$.

The single crystal X-ray structure (Fig. 18, RHS; Table 6) reveals a dinuclear bis architecture with two doubly bridging triazolate ligands equatorially bound to two iron(III) centers with four axial chlorides (two per iron) to balance the charge giving a neutral complex overall and a coordination sphere of N$_4$Cl$_2$ for each iron(III). Once again the Fe–N$_{pyridyl}$ bonds [2.200(2) Å] are longer than the Fe–N$_{triazolate}$ bonds [2.087(2) Å]. The Fe–Cl bond lengths of 2.298(1) Å and 2.300(1) Å are similar to those observed in the previous HS iron(III) structure. The 3-d pack-

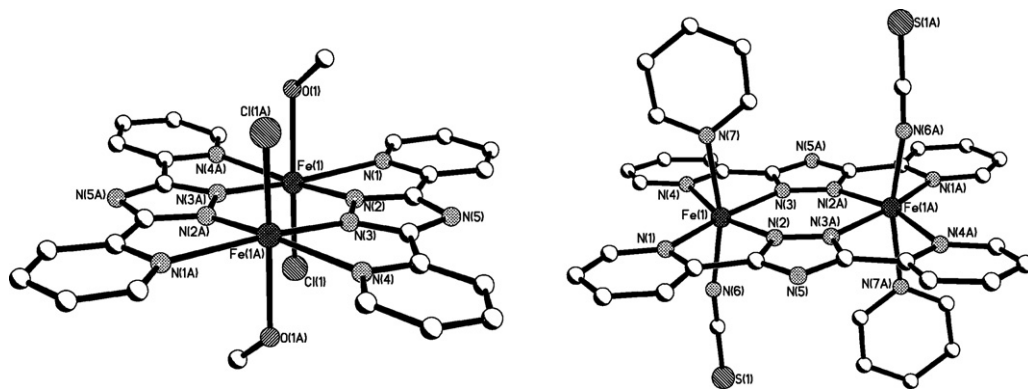Fig. 19. Structure of the two di-iron(II) complexes [Fe$_2$^{II}(**dpt**$^-$)$_2$(MeOH)$_2$Cl$_2$] at 293 K (LHS) and of [Fe$_2$^{II}(**dpt**$^-$)$_2$(py)$_2$(NCS)$_2$] at 123 K (RHS). These figures were generated from data obtained from the Cambridge Crystallographic Data Centre as published originally in [46,64].

ing of these complexes is stabilized by many weak C–H⋯Cl interactions.

3.3.2. [Fe$_2$^{II}(dpt$^-$)$_2$(MeOH)$_2$Cl$_2$]

Tong et al. also prepared dinuclear *iron(II)* complex containing **dpt**$^-$, [Fe$_2$^{II}(**dpt**$^-$)$_2$(MeOH)$_2$Cl$_2$]. This was once again a neutral complex and was prepared using an identical method and 6:1 Fe:**Hdpt** stoichiometry to that of [Fe$_2$^{II}(**dpt**$^-$)$_2$Cl$_4$] except that 6 equivalents of KSCN was added to act as a *reducing agent*, giving yellow crystals of [Fe$_2$^{II}(**dpt**$^-$)$_2$(MeOH)$_2$Cl$_2$] (79%). This complex contains two HS iron(II) centers at all temperatures studied, and they were seen to be weakly antiferromagnetically coupled with $J = -2.14$ cm^{-1}.

[Fe$_2$^{II}(**dpt**$^-$)$_2$(MeOH)$_2$Cl$_2$] crystallizes in the orthorhombic space group *Pbca*. The single crystal X-ray structure at 293 K revealed a dinuclear bis binding mode with the two iron(II) centres bridged by two **dpt**$^-$ ligands. Each iron ion also contains one axial methanol and one axial chloride giving an overall neutral complex (Fig. 19). Bond lengths and angles are consistent with those expected for HS iron(II) (Table 6). Once again Fe–N$_{pyridyl}$ bond lengths are longer than those of Fe–N$_{triazolate}$ [2.303(3) and 2.336(4) Å versus 2.108(3) and 2.113(3) Å respectively]. Overall, as expected, the bond lengths in [Fe$_2$^{II}(**dpt**$^-$)$_2$(MeOH)$_2$Cl$_2$] are longer than those in the iron(III) complex [Fe$_2$^{III}(**dpt**$^-$)$_2$Cl$_4$] (Table 6). The structure is stabilized by a hydrogen bond between the coordinated methanol O–H and the **dpt**$^-$ N^4

nitrogen atom on an adjacent molecule [O⋯N(5) = 2.745(4) Å, O–H⋯N(5) = 173(6)°]. This intermolecular hydrogen bond also facilitates the extending of the structure into a two dimensional architecture.

3.3.3. [Fe$_2$^{II}(dpt$^-$)$_2$(py)$_2$(NCX)$_2$] family

Dinuclear iron(II) structures incorporating **dpt**$^-$ were also synthesised by Murray and co-workers [64]. The key difference between these and Tong's **dpt**$^-$ complexes is that in Murray's, the iron(II) centre has an N$_6$ coordination sphere, the optimal arrangement to achieve SCO. Three complexes were prepared in which the triazolate ligand **dpt**$^-$ bridges two iron(II) centers, and the remainder of the coordination sphere for each iron(II) is made up with a pyridine and either NCS, NCSe or NCBH$_3$ giving the overall formula [Fe$_2$^{II}(**dpt**$^-$)$_2$(py)$_2$(NCX)$_2$]. Only the structure of [Fe$_2$^{II}(**dpt**$^-$)$_2$(py)$_2$(NCS)$_2$] was obtained, however reference will be made to the magnetic properties of the other complexes also.

All three complexes were prepared under a nitrogen atmosphere. [Fe$_2$^{II}(**dpt**$^-$)$_2$(py)$_2$(NCS)$_2$] was made by adding [(*n*-Bu)$_4$N](**dpt**$^-$) (1 equivalent) in pyridine to a stirred solution of 1 equivalent of [Fe^{II}(py)$_4$(NCS)$_2$] in methanol, giving a yellow solution with a yellow precipitate. This was collected giving [Fe$_2$^{II}(**dpt**$^-$)$_2$(py)$_2$(NCS)$_2$] as a yellow microcrystalline solid in 66% yield. A slightly different approach was used

Table 6
Selected bond lengths and angles for [Fe^{III}$_2$(**dpt**$^-$)$_2$Cl$_4$] at 293 K and for [Fe$_2$^{II}(**dpt**$^-$)$_2$(MeOH)$_2$Cl$_2$] at 293 K

Bond lengths (Å) and angles (°)	[Fe$_2$^{III}(**dpt**$^-$)$_2$Cl$_4$]	Bond lengths (Å) and angles (°)	[Fe$_2$^{II}(**dpt**$^-$)$_2$(MeOH)$_2$Cl$_2$]
Fe–N$_P$	2.200(2)	Fe–N$_P$	2.336(4)
Fe–N$_T$	2.087(2)	Fe–N$_T$	2.108(3)
Fe–Cl$_1$	2.298(1)	Fe–N$_T$*	2.113(3)
Fe–Cl$_2$	2.300(1)	Fe–N$_P$*	2.303(3)
Fe–Fe	4.408(2)	Fe–Cl	2.343(1)
		Fe–O	2.205(3)
		Fe–Fe	4.241
Cis-angles	75.40(7)–123.1(1)	*Cis*-angles	72.4(1)–119.0(1)
Trans-angles	159.64(4)–161.49(8)	*Trans*-angles	162.8(1)–165.2(1)
Cis-N$_P$–Fe–N$_T$	75.40(7)	*Cis*-N$_P$–Fe–N$_T$	72.4(1)
		Cis-N$_P$*–Fe–N$_T$*	73.0(1)

Symmetry operation to generate equivalent atoms: (*) $-x + 2, -y, -z + 1$.
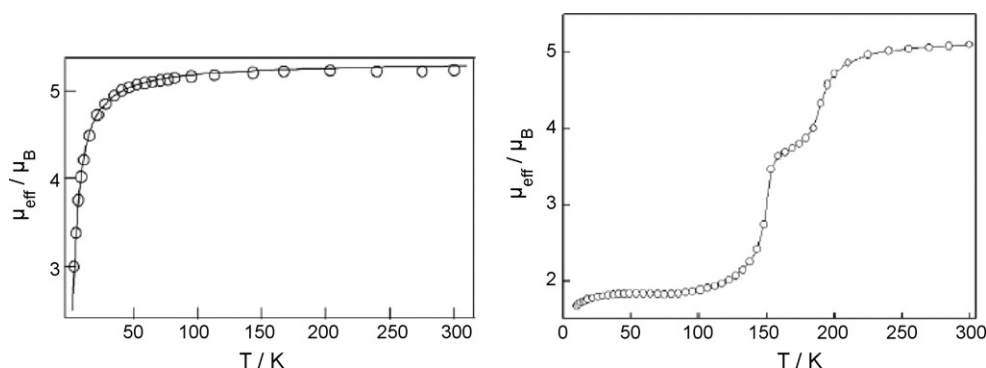
Fig. 20. Variable temperature magnetic data for [Fe_2^{II}(**dpt**$^-$)$_2$(py)$_2$(NCS)$_2$] (LHS) and [Fe_2^{II}(**dpt**$^-$)$_2$(py)$_2$(NCBH$_3$)$_2$] (RHS). Reprinted with permission from Polyhedron 26 (2007) 1764. Copyright 2007, Elsevier.

for [Fe_2^{II}(**dpt**$^-$)$_2$(py)$_2$(NCSe)$_2$] in that one equivalent of Fe(ClO$_4$)$_2$·6H$_2$O was reacted with two equivalents of KNCSe in methanol. Added to the resulting clear solution was a pyridine solution of [(n-Bu)$_4$N](**dpt**$^-$) (1 equivalent) giving the desired product as a yellow precipitate in 39% yield. The preparation of [Fe_2^{II}(**dpt**$^-$)$_2$(py)$_2$(NCBH$_3$)$_2$] also used a slightly different method in that FeSO$_4$·7H$_2$O (1 equivalent) and Na(NCBH$_3$) (2 equivalents) were reacted in methanol resulting in a purple solution with a precipitate of Na$_2$SO$_4$ which was filtered. To this solution was added pyridine (so that the initially formed [Fe^{II}(py)$_4$(NCBH$_3$)$_2$] dissolved) and then [(n-Bu)$_4$N](**dpt**$^-$) (1 equivalent) in pyridine. The resulting orange solution was allowed to evaporate to ∼2/3 of its original volume under nitrogen for three days, giving the desired product as fine orange needles in 42% yield.

The magnetic properties of [Fe_2^{II}(**dpt**$^-$)$_2$(py)$_2$(NCS)$_2$] and [Fe_2^{II}(**dpt**$^-$)$_2$(py)$_2$(NCSe)$_2$] show that they both contain iron(II) centres in a HS–HS arrangement with μ_{eff} = ∼5.2 μ_B for both complexes, between the temperature range 300–50 K (Fig. 20). Interestingly, when a stronger field axial co-ligand (NCBH$_3^-$) is used an SCO event occurs. The magnetic profile for [Fe_2^{II}(**dpt**$^-$)$_2$(py)$_2$(NCBH$_3$)$_2$] shows a two-step crossover from the HS–HS state [μ_{eff} = 5.0 μ_B per Fe(II)] with T_1 = 194 K to a plateau region [μ_{eff} = 3.8 μ_B per Fe(II)] extending over the temperature range 188–163 K (Fig. 20). A second SCO event occurs between 160–120 K (T_2 = 151 K) where μ_{eff} drops to 1.8 μ_B per Fe(II). The nature of the complex in the plateau region cannot be determined (i.e. is it HS–LS or a 50:50 mixture of HS–HS:LS–LS) without a crystal structure.

[Fe_2^{II}(**dpt**$^-$)$_2$(py)$_2$(NCS)$_2$] crystallizes in the monoclinic $P2_1/n$ space group and the structure was obtained at 123 K (Fig. 19, Table 7). The structure reveals a complex similar to that seen by Tong et al in that it contains two iron(II) centers bridged by two **dpt**$^-$ ligands in the equatorial positions with the remainder of the octahedral coordination sphere being completed by two axial NCS$^-$ anions and two pyridine molecules [one of each per iron(II) centre] [46]. Bond lengths range from 2.087(4)–2.330(3) Å, and *cis*-N–Fe–N bond angles from 73.34–121.63°, characteristic of HS iron(II). Once again the Fe–N$_{pyridyl}$ bond lengths are longer than those of the Fe–N$_{triazolate}$ [2.309(3) and 2.330(3) Å versus 2.119(3) and 2.121(4) Å respectively]. The iron–iron sepa-

ration in this complex is 4.34 Å, similar to that seen in Tong et al.'s dinuclear structures [46]. The crystal structure of [Fe_2^{II}(**dpt**$^-$)$_2$(NCS)$_2$(py)$_2$] reveals that it is structurally very similar to the related 3,5-di(2-pyridyl)-pyrazolate complex [Fe_2^{II}(**L**$^-$)$_2$(NCS)$_2$(py)$_2$], the structure of which was also determined in this study by Murray and co-workers, but which was first synthesised earlier by Nakano et al. [75].

There are no uncoordinated solvent molecules present within this crystal structure and no uncoordinated counter anions, thus there is no significant hydrogen bonding. Instead the structure is stabilized by π–π interactions between the π-system of the pyridyl rings and that of the triazolate ring of a neighbouring molecule (distance of 3.353 Å). This induces the formation of chains of molecules linked by these interactions. These chains are further arranged to form near perpendicular layers via edge to edge π–π stacking of the pyridyl rings (similar to that seen in a related pyrazolate structure) [75].

3.4. Comparisons and concluding remarks

A hydrothermal synthesis led to the crystallization of a mono-iron(III) complex of a unique zwitterionic form of the neutral 3,5-di(2-pyridyl) triazole ligand (**Hdpt**).

Table 7
Selected bond lengths and angles for [Fe_2^{II}(**dpt**$^-$)$_2$(py)$_2$(NCS)$_2$] at 123 K

Bond lengths (Å) and angles (°)	[Fe_2^{II}(**dpt**$^-$)$_2$(py)$_2$(NCS)$_2$]
Fe–N$_P$	2.330(3)
Fe–N$_T$	2.119(3)
Fe–N$_T$*	2.121(4)
Fe–N$_P$*	2.309(3)
Fe–N$_X$	2.087(4)
Fe–N$_P$†	2.220(4)
Fe–Fe	4.340(3)
Cis-N–Fe–N	73.34(12)–121.63(12)
Trans-N–Fe–N	163.81(13)–165.31(14)
Cis-N$_P$–Fe–N$_T$	73.34(12)
Cis-N$_P$*–Fe–N$_T$*	73.54(13)
Fe–N$_X$–C$_X$	169.3(3)

N$_P$† = axial pyridine nitrogen donor atom. Symmetry operation to generate equivalent atoms: (*) $-x+1$, $-y$, $-z+2$.

In contrast, the 3,5-di(2-pyridyl) tria<u>zolate</u> ligand **dpt$^-$** has facilitated the isolation of the first examples of structurally characterized *dinuclear* iron complexes. Indeed no mononuclear iron complexes of **dpt$^-$** have been reported to date. Whether this is due to it being far more electron rich, and hence more able to bind to more than one metal ion, than the neutral analogues, or whether it is more to do with the significant change in solubility, or other as yet unidentified factors, is not yet clear as the number of studies performed to date is so small. It is intriguing that *both di-iron(II) and di-iron(III)* complexes of this triazolate ligand can be obtained. In contrast, the neutral triazoles described in Section 2 generated exclusively *mononuclear iron(II)* complexes.

One might have expected that the negatively charged triazolate ligands might lead to rather ready oxidation of iron(II) to iron(III), making the isolation of the, more magnetically interesting, iron(II) complexes problematic. Clearly this is not an insurmountable problem as both the hydrothermal method of Tong et al., using 6 equivalents of sacrificial KSCN as reducing agent (no NCS$^-$ coordinated in product), and the Schlenk techniques used by Murray and co-workers have proven successful in this regard.

The magnetic properties of the dinuclear complexes are of considerable interest, as if they are SCO-active they are able to exist in three states, [HS–HS], ["HS–LS"] and [LS–LS]. This three state switching was seen by Murray and co-workers for [Fe$_2^{II}$(**dpt$^-$**)$_2$(NCBH$_3$)$_2$(py)$_2$]. In that case the exact nature of the "half SCO" species, ["HS–LS"], i.e. whether it is [HS–LS] or 1:1 [HS–HS]:[LS–LS], was not determined. No X-ray crystal structure or in depth Mössbauer study was reported.

4. Conclusions

N^4-substituted/unsubstituted-3,5-di(2-pyridyl)-1,2,4-triazole/triazolates are an exciting class of ligands producing magnetically interesting complexes when reacted with iron, as the field strength of such azole containing ligands is often in the appropriate range to give SCO in iron(II).

A summary of key information for all of the complexes discussed in this review is provided in Table 1. It draws attention to the crystal structure, binding modes, colour, yield, oxidation state and magnetic properties. The table allows one to easily view the impact that subtle and not-so-subtle changes to the complex have on the magnetic properties, in particular the SCO behaviour.

While in principle the neutral 3,5-di(2-pyridyl)-1,2,4-triazole ligands have two bidentate binding pockets available, they have not given any dinuclear iron complexes to date, rather they have led exclusively to mononuclear iron complexes. Despite this they have been shown to facilitate the preparation of interesting SCO compounds. This is nicely illustrated by the fact that of the 9 structurally characterized complexes of N^4-*substituted* 3,5-di(2-pyridyl)-1,2,4-triazole ligands [all mononuclear iron(II)] all but two of them are SCO active. Interestingly, of the many such ligands currently available, with differing N^4-substituents (Fig S1, ESI), only four ligands (Fig. 1) have been reacted with iron to date. Another interesting point is that iron complexes in which the exact nature of the 2-pyridyl rings has been fine-tuned, for example by the introduction of additional substituents, have not yet been reported. In principle this would allow steric, electronic, packing, etc. effects to be probed. One structurally characterized copper complex exists in which one of the 2-pyridyl rings contains a methyl group at the 3-position, however this was not intentionally made. Rather, the triazolate ring in this complex was formed via a catalytic dehydration reaction when the initial ligand of interest was reacted with copper nitrate [14]. As an aside, synthetic pathways now exist that should also allow access to other heterocycles being incorporated at the C^3 and C^5 positions of such ligands [10].

Conveniently, given that the focus is on SCO in iron(II) complexes of these ligands, no iron(III) complexes have been produced from the N^4-substituted (neutral) 3,5-di(2-pyridyl)-1,2,4-triazole ligands. In contrast the zwitterionic form of the N^4-*unsubstituted* ligand **Hdpt** did give a HS mononuclear iron(III) complex.

The (N^4-unsubstituted) 3,5-di(2-pyridyl)-1,2,4-tria<u>zolate</u> ligands have shown very different behaviour, generating exclusively *dinuclear* iron complexes to date. Presumably the greater electron density on the negatively charged triazolate ring facilitates binding to two, not just to one, iron centre. However, at this stage it is hard to rule out the importance of stoichiometry, solvent choice etc. to the nature of the product obtained. Both di-iron(II) and di-iron(III) complexes have been formed. That iron(III) complexes are readily formed is understandable considering that the ligands have a negative charge, and thus will favour higher oxidation states of transition metal ions. It is however good to see that an appropriate choice of reaction conditions still allows one to cleanly isolate the iron(II) complexes of interest. To date, only one complex, the dinuclear complex [Fe$_2^{II}$(**dpt$^-$**)$_2$(py)$_2$(NCBH$_3$)$_2$], has been found to be

---

Table 8

Average bond-lengths and *cis*-N$_P$–Fe–N$_T$ angles (with ranges) for the iron(II) complexes of tria*zoles* (all *mononuclear*) and tria*zolates* (all *dinuclear*)

	Triazole (nine HS structures)	Triazolate (two HS structures)[a]
Average Fe–N$_P$ (Å)	2.248	2.319
Fe–N$_P$ range (Å)	2.12–2.252	2.303–2.336
Average Fe–N$_T$ (Å)	2.154	2.115
Fe–N$_T$ range (Å)	2.08–2.248	2.108–2.121
Average *cis*-N$_P$–Fe–N$_T$ (°)	74.85	73.07
Cis-N$_P$–Fe–N$_T$ range (°)	74.17–77.2	72.4–73.54

[a] Each of these dinuclear structures has two sets of relevant bond lengths.

SCO active. It underwent a two-step SCO event, making it one of the most magnetically interesting complexes in this review; however the lack of a crystal structure or detailed Mössbauer analysis means that the exact nature of the half crossover species is yet to be determined.

There are 11 structures of HS iron(II) complexes, 9 of which are *mononuclear* complexes of triazoles and 2 of which are *dinuclear* complexes of triazolates. The Fe–N$_{pyridine}$ versus Fe–N$_{triazole/triazolate}$ bond lengths in these HS iron(II) triazole (9) and triazolate (2) complexes have been compared (Table 8). Given the small number of such structures and the differences in structural types these comparisons are tentative only. On average, the Fe–N$_{pyridine}$ bond is longer than that of the N$_{triazole/triazolate}$ bond. Indeed only one case, that of *cis* [Fe^{II}(***m-mdpt***)$_2$(NCS)$_2$] was the reverse situation found, probably for steric reasons. The average Fe–N$_{pyridine}$ bond length for the mononuclear triazole complexes is seen to be 2.248 Å while in the dinuclear triazolate complexes it is seen to be significantly longer, 2.319 Å. In contrast, as might be expected, the average Fe–N$_{triazole/triazolate}$ bond length is somewhat longer, 2.154 Å, in the mononuclear triazole complexes than in the dinuclear triazolate complexes, 2.115 Å. The *cis*-N$_P$–Fe–N$_T$ bond angle is somewhat more acute in the dinuclear triazolate structures than in the mononuclear triazole structures. There are only 2 LS structures of iron(II) complexes and both are *mononuclear* complexes of triazole ligands. As expected, due to changes in d orbital occupancies from HS to LS, both sets of bond lengths are significantly shorter in these LS structures: Fe–N$_{pyridine}$ = 2.02, 2.028 (average 2.024 Å; 0.224 Å shorter than the 9 HS mononuclear triazoles) and Fe–N$_{triazole}$ = 2.00, 1.983 (average 1.991 Å; 0.163 Å shorter than the 9 HS mononuclear triazoles), and the *cis*-N$_P$–Fe–N$_T$ angles are closer to 90° (80.3°, 80.5°).

Acknowledgement

Appendix A. Supplementary data

Supplementary data associated with this article can be found, in the online version, at doi:10.1016/j.ccr.2007.11.010.

Note

The search of the Cambridge Structural Database employed CSD version 5.28 updates Jan 2007 [76,77].

References

[1] P. Gütlich, H.A. Goodwin, Top. Curr. Chem. 233 (2004) 1.
[2] P.J. van Koningsbruggen, Top. Curr. Chem. 233 (2004) 123.
[3] P. Gütlich, Y. Garcia, H.A. Goodwin, Chem. Soc. Rev. 29 (2000) 419.
[4] O. Kahn, C.J. Martinez, Science (Washington D.C.) 279 (1998) 44.
[5] J.G. Haasnoot, 1,2,4-Triazoles as Ligands for Iron(II) High Spin-low Spin Crossovers, Kluwer Academic Publishers, Dordrecht, 1996.
[6] P. Gütlich, Struct. Bond. 44 (1981) 83.
[7] H.A. Goodwin, P. Gütlich, Top. Curr. Chem. 233 (2004) 1.
[8] J.F. Geldard, F. Lions, J. Org. Chem. 30 (1965) 318.
[9] M.H. Klingele, S. Brooker, Coord. Chem. Rev. 241 (2003) 119.
[10] M.H. Klingele, S. Brooker, Eur. J. Org. Chem. (2004) 3422.
[11] M.H. Klingele, B. Moubaraki, K.S. Murray, S. Brooker, Chem. Eur. J. 11 (2005) 6962.
[12] C.D. Brandt, J.A. Kitchen, U. Beckmann, N.G. White, G.B. Jameson, S. Brooker, Supramol. Chem. 19 (2007) 17.
[13] M.H. Klingele, B. Moubaraki, J.D. Cashion, K.S. Murray, S. Brooker, Chem. Commun. (2005) 987.
[14] L. Zhao, C.J. Matthews, Z. Xu, L.K. Thompson, D.O. Miller, Mol. Cryst. Liq. Cryst. Liq. Cryst. Sci. Technol., Sect. A 376 (2002) 386.
[15] K.H. Sugiyarto, D.C. Craig, A.D. Rae, H.A. Goodwin, Aust. J. Chem. 48 (1995) 35, and references therein.
[16] L.S. Harimanow, K.H. Sugiyarto, D.C. Craig, M.L. Scudder, H.A. Goodwin, Aust. J. Chem. 52 (1999), 109, and references therein.
[17] B.A. Leita, B. Moubaraki, K.S. Murray, J.P. Smith, Polyhedron 24 (2005), 2165, and references therein.
[18] S. Kaizaki, K. Nakano, N. Suemura, K. Yoneda, S. Kawata, Dalton Trans. (2005), 740, and references therein.
[19] J.A. Kitchen, N.G. White, B. Moubaraki, K.S. Murray, P.D.W. Boyd, S. Brooker, in preparation.
[20] O. Roubeau, M. de Vos, A.F. Stassen, R. Burriel, J.G. Haasnoot, J. Reedijk, J. Phys. Chem. Solids 64 (2003), 1003, and references therein.
[21] J.-P. Zhang, Y.-Y. Lin, X.-C. Huang, X.-M. Chen, Chem. Commun. (2005) 1258.
[22] G. Yucesan, M.H. Yu, W. Ouellette, C.J. O'Connor, J. Zubieta, Cryst. Eng. Comm. 7 (2005) 480.
[23] J.-C. Chen, A.-J. Zhou, S. Hu, M.-L. Tong, Y.-X. Tong, J. Mol. Struct. 794 (2006) 225.
[24] S.-C. Shao, D.-R. Zhu, X.-H. Zhu, X.-Z. You, S.S.S. Raj, H.-K. Fun, Acta Crystallogr., Sect. C 55 (1999) 1412.
[25] S.-C. Shao, S.-D. Liu, H.-L. Zhu, Acta Crystallogr., Sect. E 60 (2004) m1815.
[26] F.S. Keij, R.A.G. deGraaff, J.G. Haasnoot, J. Reedijk, J. Chem. Soc., Dalton Trans. (1984) 2093.
[27] R. Prins, P.J.M.L. Birker, J.G. Haasnoot, G.C. Verschoor, J. Reedijk, Inorg. Chem. 24 (1985) 4128.
[28] M. Shakir, S. Parveen, N. Begum, Y. Azim, Polyhedron 22 (2003) 3181.
[29] U. Garcia-Couceiro, O. Castillo, A. Luque, G. Beobide, P. Roman, Acta Crystallogr., Sect. E 60 (2004) m720.
[30] D. Zhu, Y. Xu, Z. Yu, Z. Guo, H. Sang, T. Liu, X. You, Chem. Mater. 14 (2002) 838.
[31] S.-C. Shao, Z.-L. You, S.-P. Zhang, S.W. Ng, H.-L. Zhu, Acta Crystallogr., Sect. E 61 (2005) m265.
[32] S.-P. Zhang, Z.-D. Liu, J.-L. Ma, S. Yang, S.-C. Shao, Acta Crystallogr., Sect. E 61 (2005) m423.
[33] N. Moliner, A.B. Gaspar, M.C. Muñoz, V. Niel, H. Cano, J.A. Real, Inorg. Chem. 40 (2001) 3986.
[34] G.S. Matouzenko, A. Boussekou, S. Borshch, M. Perrin, S. Zein, L. Salmon, G. Molnar, S. Lecocq, Inorg. Chem. 43 (2004) 227.
[35] D. Mulhern, S. Brooker, G.H.S. Rau, J.G. Vos, Dalton Trans. (2006) 51.
[36] M.H. Klingele, P.D.W. Boyd, B. Moubaraki, K.S. Murray, S. Brooker, Eur. J. Inorg. Chem. (2006) 573.
[37] R. Hage, J.G. Haasnoot, H.A. Nieuwenhuis, J. Reedijk, D.J.A. de Ridder, J.G. Vos, J. Am. Chem. Soc. 112 (1990) 9245.
[38] S.K. Mandal, H.J. Clase, J.N. Bridson, S. Ray, Inorg. Chim. Acta 209 (1993) 1.
[39] A.L. Rheingold, P. Saisuwan, N.C. Thomas, Inorg. Chim. Acta 214 (1993) 41.
[40] P.J. Van Koningsbruggen, K. Goubitz, J.G. Haasnoot, J. Reedijk, Inorg. Chim. Acta 268 (1998) 37.
[41] S.-P. Zhang, S.-C. Shao, Z.-D. Liu, H.-L. Zhu, Acta Crystallogr., Sect. E 61 (2005) m799.
[42] N. Moliner, M.C. Muñoz, S. Letard, J.-F. Letard, X. Solans, R. Burriel, M. Castro, O. Kahn, J.A. Real, Inorg. Chim. Acta 291 (1999) 279.

[43] A.B. Gaspar, M.C. Muñoz, N. Moliner, V. Ksenofontov, G. Levchenko, P. Gütlich, J.A. Real, Monatsh. Chem. 134 (2003) 285.

[44] D.-R. Zhu, Y. Song, Y. Xu, Y. Zhang, S.S.S. Raj, H.-K. Fun, X.-z. You, Polyhedron 19 (2000) 2019.

[45] M. Shakir, S. Parveen, N. Begum, P. Chingsubam, Trans. Metal Chem. 29 (2004) 196.

[46] M.-L. Tong, Y.-X. Tong, J.-C. Chen, S. Hu, A.-J. Zhou, Z. Anorg. Allg. Chem. 632 (2006) 475.

[47] C. Faulmann, P.J. van Koningsbruggen, R.A.G. de Graaff, J.G. Haasnoot, J. Reedijk, Acta Crystallogr., Sect. C C46 (1990) 2357.

[48] J.P. Cornelissen, J.H. Van Diemen, L.R. Groeneveld, J.G. Haasnoot, A.L. Spek, J. Reedijk, Inorg. Chem. 31 (1992) 198.

[49] J.-P. Zhang, Y.-Y. Lin, X.-C. Huang, X.-M. Chen, J. Am. Chem. Soc. 127 (2005) 5495.

[50] A.J. Jircitano, S.O. Sommerer, K.A. Abboud, Acta Crystallogr., Sect. C 53 (1997) 434.

[51] F.R. Keene, D.M. D'Alessandro, P.H. Dinolfo, J.T. Hupp, P.C. Junk, Eur. J. Inorg. Chem. (2006) 772.

[52] R. Hage, J.P. Turkenburg, R.A.G. deGraaff, J.G. Haasnoot, J. Reedijk, J.G. Vos, Acta Crystallogr., Sect. C 45 (1989) 381.

[53] D. Zhu, Y. Song, Y. Liu, Y. Xu, Y. Zhang, X. You, S.S.S. Raj, H.-K. Fun, Trans. Metal Chem. 25 (2000) 589.

[54] H.M. Burke, J.F. Gallagher, M. Indelli, T.F. Scandola, J.G. Vos, Eur. J. Inorg. Chem. (2002) 846.

[55] H.M. Burke, J.F. Gallagher, M. Indelli, T.J.G. Vos, Inorg. Chim. Acta 357 (2004) 2989.

[56] D.R. Zhu, Y. Xu, Y. Mei, Y. Shi, C. Tu, X. You, J. Mol. Struct. 559 (2001) 119.

[57] M.H. Klingele, P.D.W. Boyd, B. Moubaraki, K.S. Murray, S. Brooker, Eur. J. Inorg. Chem. (2005) 910.

[58] D. Braga, M. Polito, S. Giaffreda, L.F. Grepioni, Dalton Trans. (2005) 2766.

[59] P.J. van Koningsbruggen, D. Gatteschi, R.A.G. de Graaff, J.G. Haasnoot, J. Reedijk, C. Zanchini, Inorg. Chem. 34 (1995) 5175.

[60] U. Hartmann, H. Vahrenkamp, Inorg. Chim. Acta 239 (1995) 13.

[61] P.J. Kunkeler, P.J. van Koningsbruggen, J.P. Cornelissen, A.N. van der Horst, A.M. van der Kraan, A.L. Spek, J.G. Haasnoot, J. Reedijk, J. Am. Chem. Soc. 118 (1996) 2190.

[62] Q.-G. Zhai, X.-Y. Wu, S.-M. Chen, C.-Z. Lu, W.-B. Yang, Cryst. Growth Des. 6 (2006) 2126.

[63] M.H. Klingele, A. Noble, P.D.W. Boyd, S. Brooker, Polyhedron 26 (2007) 479.

[64] C.J. Schneider, J.D. Cashion, B. Moubaraki, S.M. Neville, S.R. Batten, D.R. Turner, K.S. Murray, Polyhedron 26 (2007) 1764.

[65] N. Moliner, M.C. Muñoz, P.J. van Koningsbruggen, J.A. Real, Inorg. Chim. Acta 274 (1998) 1.

[66] S. Pillet, C. Lecompt, C.F. Sheu, Y.C. Lin, I.J. Hsu, Y. Wang, J. Phys.: Conf. Ser. 21 (2005) 221.

[67] J.-F. Letard, J. Mater. Chem. 16 (2006) 2550.

[68] J.-F. Letard, P. Guionneau, L. Rabardel, J.A.K. Howard, A.E. Goeta, D. Chassaeu, O. Kahn, Inorg. Chem. 37 (1998) 4432.

[69] A. Desaix, O. Roubeau, J. Jeftic, J.G. Haasnoot, K. Boukheddaden, E. Codjovi, J. Linares, M. Nogues, F. Varret, Eur. Phys. J. B 6 (1998) 183.

[70] J.A. Real, A.B. Gaspar, V. Niel, M.C. Muñoz, Coord. Chem. Rev. 236 (2003) 121.

[71] O. Roubeau, J.M.A. Gomez, E. Balskus, J.J.A. Kolnaar, J.G. Haasnoot, J. Reedijk, New J. Chem. 25 (2001) 144.

[72] W.A. Baker Jr., G.J. Long, J. Chem. Soc., Chem. Commun. (1965) 368.

[73] P. Coronel, A. Barraud, R. Claude, O. Kahn, A. Ruadel-Teixier, J. Zarembowitch, J. Chem. Soc., Chem. Commun. (1989) 193.

[74] A.B. Gaspar, M.C. Muñoz, J.A. Real, J. Mater. Chem. 16 (2006) 2522.

[75] K. Nakano, N. Suemura, S. Kawata, A. Fuyuhiro, T. Yagi, S. Nasu, S. Morimoto, S. Kaizaki, Dalton Trans. (2004) 982.

[76] F.H. Allen, S.A. Bellard, M.D. Brice, B.A. Cartwright, A. Doubleday, H. Higgs, T. Hummelink, B.G. Hummelink-Peters, O. Kennard, W.D.S. Motherwell, J.R. Rodgers, D.G. Watson, Acta Crystallogr., Sect. B 35 (1979) 2331.

[77] F.H. Allen, Acta Crystallogr., Sect. B 58 (2002) 380.